Low-Cost Sensors and Multitemporal Remote Sensing for Operational Turbidity Monitoring in an East African Wetland Environment

Stefanie Steinbach, Andreas Rienow, Martin Wainaina Chege, Niels Dedring, Wisdom Kipkemboi, Bartholomew Kuria Thiong'o, Sander Jaap Zwart, and Andrew Nelson

***Abstract*—Many wetlands in East Africa are farmed and wetland reservoirs are used for irrigation, livestock, and fishing. Water quality and agriculture have a mutual influence on each other. Turbidity is a principal indicator of water quality and can be used for, otherwise, unmonitored water sources. Low-cost turbidity sensors improve in situ coverage and enable community engagement. The availability of high spatial resolution satellite images from the Sentinel-2 multispectral instrument and of bio-optical models, such as the Case 2 Regional CoastColor (C2RCC) processor, has fostered turbidity modeling. However, these models need local adjustment, and the quality of low-cost sensor measurements is debated. We tested the combination of both technologies to monitor turbidity in small wetland reservoirs in Kenya. We sampled ten reservoirs with low-cost sensors and a turbidimeter during five Sentinel-2 overpasses. Low-cost sensor calibration resulted in an R^2 of 0.71. The models using the C2RCC C2X-COMPLEX (C2XC) neural nets with turbidimeter measurements ($R^2 = 0.83$) and with low-cost measurements ($R^2 = 0.62$) performed better than the turbidimeter-based C2X model. The C2XC models showed similar patterns for a one-year time series, particularly around the turbidity limit set by Kenyan authorities. This shows that both the data from the commercial turbidimeter and the low-cost sensor setup, despite sensor uncertainties, could be used to validate the applicability of C2RCC in the study area, select the better-performing neural nets, and adapt the model to the study site. We conclude that combined monitoring with low-cost sensors and remote sensing can support wetland and water management while strengthening community-centered approaches.**

***Index Terms*—Agricultural water management, Case 2 Regional CoastColor (C2RCC), Sentinel-2, water quality.**

Manuscript received 10 October 2023; revised 22 February 2024; accepted 16 March 2024. Date of publication 27 March 2024; date of current version 22 April 2024. This work was supported in part by the German Federal Ministry of Education and Research (BMBF) through the Project "Participatory Approach to Environmental Conservation of the Muringato Catchment Area for Sustainable Management and Enhanced Ecosystem Health" (CITGI4Muringato) under Grant Agreement No. 01DG20022 and in part by the DFG Open Access Publication Fund of the Ruhr University Bochum. *(Corresponding author: Stefanie Steinbach.)*

Stefanie Steinbach is with the Institute of Geography, Ruhr University Bochum, 44801 Bochum, Germany, and also with the Faculty of Geo-Information Science and Earth Observation (ITC), University of Twente, 7522 NH Enschede, The Netherlands (e-mail: stefanie.steinbach@rub.de, s.steinbach@utwente.nl).

Andreas Rienow and Niels Dedring are with the Institute of Geography, Ruhr University Bochum, 44801 Bochum, Germany (e-mail: andreas.rienow@rub.de; niels.dedring@rub.de).

Martin Wainaina Chege, Wisdom Kipkemboi, and Bartholomew Kuria Thiong'o are with the Institute of Geomatics, GIS and Remote Sensing, Dedan Kimathi University of Technology, Nyeri 10143, Kenya (e-mail: martin.chege17@students.dkut.ac.ke; wisdom.kipkemboi21@students.dkut.ac.ke; kuria.thiongo@dkut.ac.ke).

Sander Jaap Zwart is with the International Water Management Institute, Accra PMB CT 112, Ghana (e-mail: s.zwart@cgiar.org).

Andrew Nelson is with the Faculty of Geo-Information Science and Earth Observation (ITC), University of Twente, 7522 NH Enschede, The Netherlands (e-mail: a.nelson@utwente.nl).

Digital Object Identifier 10.1109/JSTARS.2024.3381756

I. Introduction

LOW costs, simplicity, and adaptability to local conditions have entailed the construction of thousands of small reservoirs across the African continent [1], [2]. There is no comprehensive inventory, but up to 95% of all African reservoirs may be small with a surface area below 100 ha and up to 59% are below 10 ha [3]. Although their performance in terms of water availability and productivity varies strongly [4], they can support smallholder agriculture and farmer-led irrigation development [5], [6]. Wetland cultivation and damming are common across East Africa [7], [8], [9]. The use of wetlands significantly determines water quality in small reservoirs [10], [11]. Likewise, water quality critically impacts the ecological status and functioning of wetlands [12], [13].

The density of water quantity and quality monitoring locations is substantially lower in Africa compared with other continents, and even more for small water bodies [13]. Traditional monitoring methods require physical access to the water body and they do not produce spatially continuous data, which is why remote sensing has been proposed as a cost-effective alternative for spatially and temporally continuous water quality monitoring [14], [15]. Different methods and models for water quality monitoring exist and are widely used but require more validation over inland water bodies under different environmental scenarios [16], [17].

Various studies have shown how remote-sensing observations can be matched with ground reference data to derive different water quality parameters [14], [18], [19], [20], [21], [22]. Remote-sensing observations can capture optically active constituents, such as chlorophyll-*a* (Chl-*a*) as an indicator of phytoplankton [23], colored dissolved organic matter (CDOM) [24], and total suspended matter (TSM) as a measure of particle load [25]. Like TSM, turbidity refers to suspended particles but is measured as a function of light scattering by particles in the water. Light attenuation and scattering factors, such as the shape, size, and color, as well as interactions with other optically active

constituents in addition to particle mass, influence turbidity [26]. For ground measurements, turbidity is often preferred over TSM for quick assessments, as it can be easily measured with a portable or stationary turbidimeter [26], [27]. Bio-optical modeling refers to the analysis of the water status based on light absorption and scattering as a result of the concentrations and interactions of optically active constituents [28]. Empirical models for inland water bodies establish statistical relationships between water leaving radiance from one or more bands, band ratios, or band arithmetic to one or more inherent optical properties (IOPs) [19]. However, such models are usually difficult to transfer to other sites or sensors. In contrast, advanced semianalytical models are characterized by their greater robustness due to the combination of physical assumptions with the training on large remote sensing and ground databases [14], [19], [29], [30]. The launch of satellites that provide publicly available high spatial resolution imagery, such as Sentinel-2 multispectral instrument (MSI) data, has stimulated a growth in studies that use various model types for extracting optically active constituents of small water bodies [31], [32], [33].

In situ measurements are necessary for model calibration and validation and, therefore, represent a major bottleneck [14]. Water quality sampling in the field can be complex and cost-intensive [31]. An inexpensive option to determine water clarity is Secchi disk depth, which only requires a white disk that is lowered into the water until the surveyor cannot discern it anymore. However, this method is subjective to the surveyor's interpretation and is not always feasible under field conditions [18], [34]. Low-cost sensor technology has gained attention in various scientific fields, including water quality monitoring [35], [36]. The opportunities of their use to promote citizen engagement in environmental processes [37] and to increase ground observations in data-scarce environments have been widely discussed [37], [38], [39]. Commercial off-the-shelf turbidity sensors are the third most frequently researched low-cost sensors in scientific water quality studies, after pH and temperature sensors. However, the developed systems are often not calibrated against professional equipment or lack calibration and validation altogether [40]. Low-cost turbidity sensors have been used in various water quality monitoring approaches [41], [42], [43] and, in one instance, water quality smartphone apps compared with satellite-derived information [44]. Yet, to the best of our knowledge, the potential of combining remote sensing and low-cost sensor technology to validate a locally adapted remote-sensing-based turbidity model has not been evaluated.

This study aims to address the challenge of spatially and temporally continuous water quality monitoring in small tropical wetland reservoirs with low-cost sensor technology and satellite remote sensing. The objectives are as follows:

1) to calibrate and assess the performance of two low-cost turbidity sensor types under field conditions;
2) to calibrate and apply remote-sensing turbidity models based on Sentinel-2 MSI imagery, processed with the semianalytical Case 2 Regional CoastColor (C2RCC) processor [30], and parameterized with turbidimeter and low-cost sensor ground measurements;
3) to evaluate the turbidity retrieval approach with respect to national water quality guidelines and to the potentials of technology integration in operational turbidity monitoring.

To achieve these objectives, we selected ten small reservoirs located in wetlands in Nyeri county, Kenya, where we conducted a sampling campaign, using both laboratory equipment and low-cost sensors to measure turbidity. We matched field observations with Sentinel-2 imagery and derived turbidity time series for the reservoirs. Our study contributes to a better understanding of the potentials of remote-sensing-based turbidity modeling and of low-cost turbidity sensors for operational monitoring of water quality in wetland reservoirs.

II. Study Area

The study area is located in the upper Tana basin between 36.908° and 37.089° E and 0.356° and 0.444° S in Nyeri county in the central Kenyan highlands. It is about 300 km^2 in size and spans an elevation from 1700 to 1900 m a.s.l. (see Fig. 1). The long rains are from early March to the end of May and the short rains occur between the end of September and early January [45]. Recent research indicates that land-cover change over the past 30 years, including considerable deforestation and cropland and rangeland expansion, has decreased evapotranspiration and increased runoff, which can impact available water resources [46]. Farmers cultivate crops and graze livestock in small inland valley wetlands, defined as land area that is permanently or seasonally saturated with water and supports a distinct ecosystem. The wetland reservoirs form community-managed, integrated water-agriculture systems [47]. The share of wetland cover in Nyeri county has declined from 0.07% to 0.04% between 1990 and 2014 [48]. Insufficient data on the location of water features and their quality, illegal abstraction, and the lack of public awareness are prevailing water management problems [47]. Goebel et al. [49] address the data gap with improved remote-sensing mapping methods and Kipkemboi et al. [50] through a community Web–GIS platform for environmental monitoring. Since the Water Act 2016, Kenya has decentralized water management and shifted to a community-based approach through water resources user associations (WRUAs) [51]. The wetlands and reservoirs in the study area, with the exception of one privately operated, fall under the WRUA management scheme.

Small reservoirs in the study area were identified using Google Earth and characterized during a presurvey (see Fig. 1). During the main field campaign in January 2023, water depth was measured with a sonar and the maximum added to the reservoir information (see Table I). The surface area was estimated from very high spatial resolution Google Earth imagery from August 2022. The most common reservoir uses are irrigation, livestock watering, fishing, and recreation. The reservoirs have surface areas ranging from 0.45 to 5.61 ha and are shallow with maximum depths between under 1 and 4 m. According to the respective responsible community members, all of the reservoirs are prone to siltation.

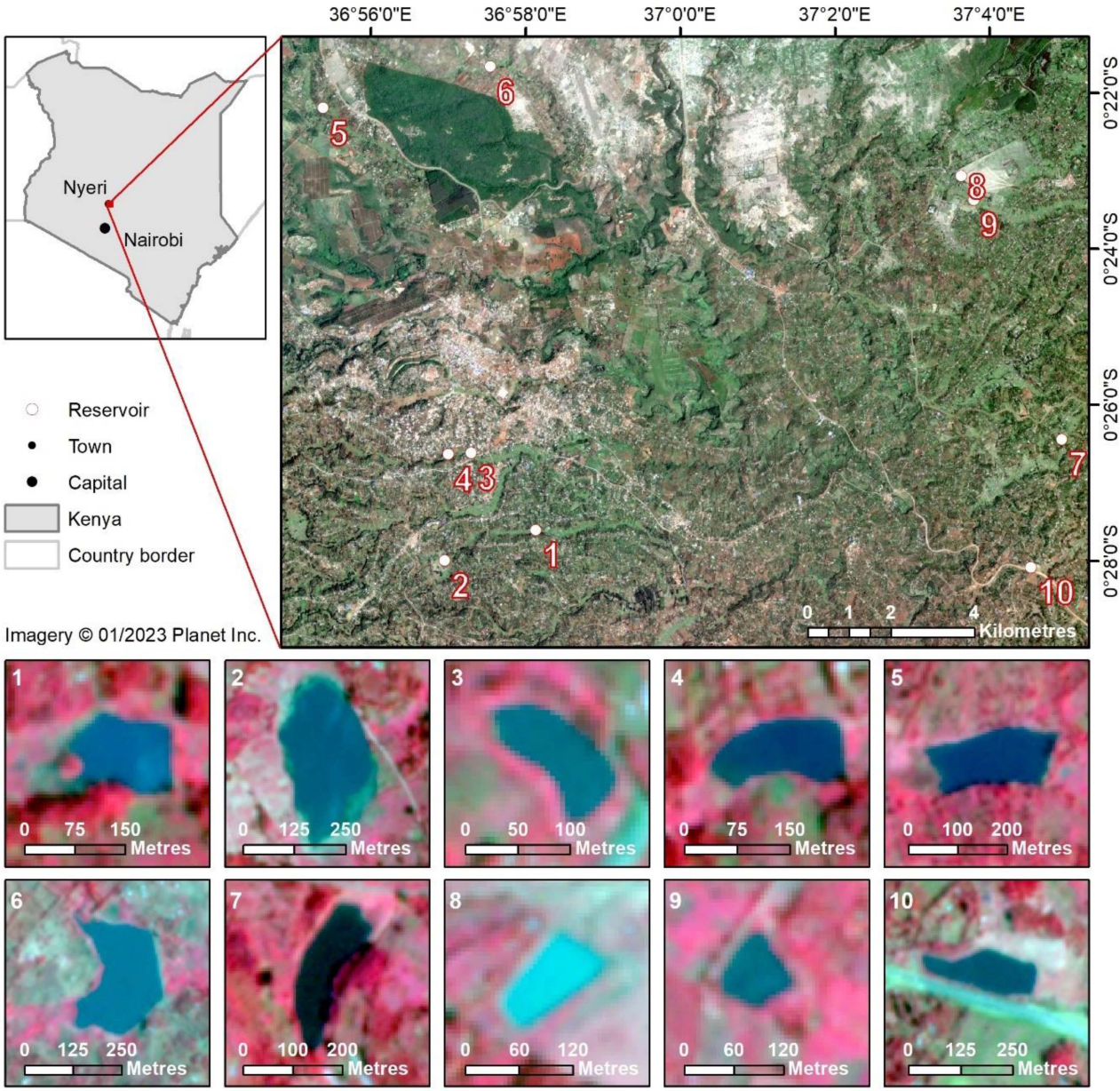

Fig. 1. Identified reservoirs in the study area in central Kenya, which are located in inland valley wetlands, that intersperse the area in narrow bands of green, with close-ups of the reservoirs in false-color Planet best-pixel composite from January 2023 (NIR-R-G).

III. Materials and Methods

This study comprised remote-sensing analysis, in situ water sampling, low-cost sensor calibration, and turbidity model parameterization, as shown in Fig. 2.

A. In Situ Turbidity Measurements

1) Water Sampling: We conducted water quality measurements to match the dates of five Sentinel-2 overpasses in January 2023 (see Table II). The sampling was carried out on two days within a timeframe of ± 1 day of each overpass to increase the sample size [52], [53]. For each round, we sampled at inflow, center, and outflow locations (c.f. Fig. 3). The dam construction varied across the sites in terms of the size of concrete installations and pipes, channeling of inflow or outflow water, and presence and extent of riparian vegetation. Where the inflow or outflow water features were not easily identifiable, we selected the locations according to the residents' information. For some reservoirs, either no inflow (Kiunyu, Kagati) or no outflow (Ithenguri), or neither inflow nor outflow water features could be identified (Hohwe). In the case of Kagati, the outflow location, an underground pipe diverting water into a depression to water livestock, was only identified during the second sampling period. For Kiunyu, the shallow outflow location stopped carrying water at the last sampling period. The sampling location in the center of each reservoir was reached with an inflatable

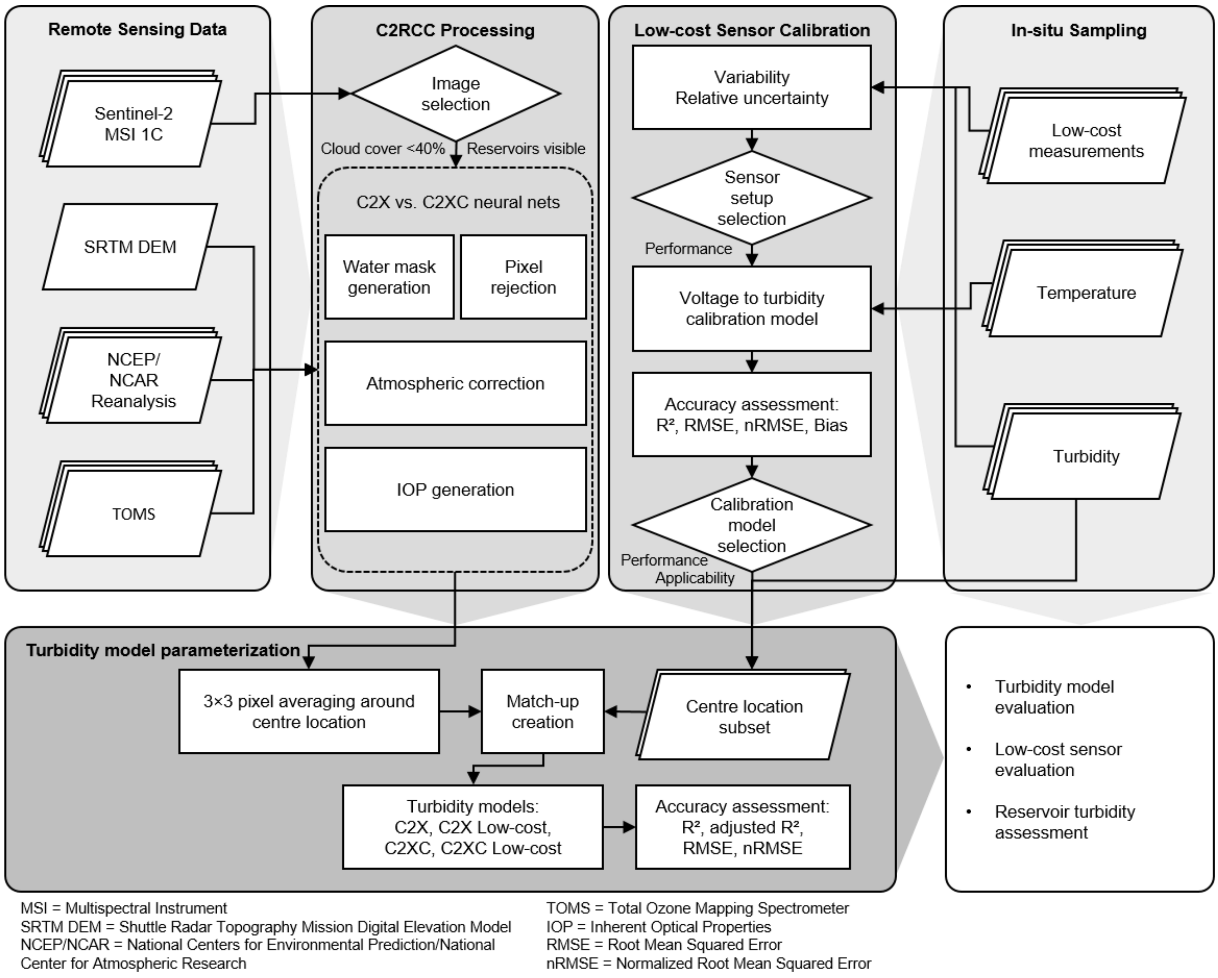

Fig. 2. Turbidity assessment workflow, including remote-sensing data processing, in situ water sampling, low-cost sensor calibration, and turbidity model parameterization.

TABLE I
INFORMATION ON THE TEN STUDIED RESERVOIRS IN NYERI COUNTY, KENYA

No.	Name	Water Uses*	Max. Depth (m)	Surface Area (ha)	Year of Construction	Ownership**
1	Ithenguri	I, F, E, R	2.1	1.36	2008	C
2	Kiunyu	I, L, F, R	<1	5.61	NA	C
3	Ndaruku	I, L, F, R	1.8	0.66	2002	C
4	Karia	I, L, F, R	2.7	1.30	2002	C
5	Njeng'u	I, L, F, R	4	2.36	1960s	C
6	Samaki	I, L, F	1.5	4.43	1975	P
7	Ruthagati	I, L, F, IP, R	4	2.06	NA	C
8	Kagati	L	1.5	0.55	2012	C
9	Hombe	I, L, F	1.8	0.45	2012	C
10	Hohwe	I, L, F	3.7	1.78	2008/ 2009	C

* I = Irrigation, F = Fishing, E = Ecotourism, R = Recreation, L = Livestock watering, and IP = Industrial processing (coffee).
** C = Community and P = Private.

TABLE II
SENTINEL-2 OVERPASS DATES AND DATES OF IN-SITU RESERVOIR SAMPLING

Overpass Date	Sampling Date	
	Reservoirs 1–4	Reservoirs 5–10
08/01/2023	08/01/2023	07/01/2023
13/01/2023	14/01/2023	13/01/2023
18/01/2023	19/01/2023	18/01/2023
23/01/2023	24/01/2023	23/01/2023
28/01/2023	28/01/2023	27/01/2023

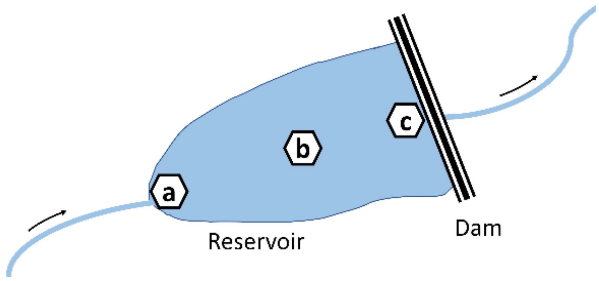

Fig. 3. Sampling locations at (a) inflow, (b) center, and (c) outflow.

kayak. The center sample was taken at about 20 cm depth. In most inland waters, the highest remote-sensing signal variability is attributed to the photic zone in the upper 1 m water layer [54]. Accordingly, sampling depths below the water surface at up to 20 cm are commonplace for inland water remote sensing [55], [56], [57]. Due to low water depth, the inflow and outflow samples were taken at the water surface. We took geolocations with a handheld Garmin eTrex 32x GPS device for all sampled locations upon the first site visit and used these as a reference for the remainder of the sampling campaign. The horizontal accuracy of the GPS device is up to 3.65 m [58]. Drift through

TABLE III
OVERVIEW OF THE WATER QUALITY PARAMETERS TAKEN AT EACH LOCATION, THEIR MEASUREMENT UNITS, DEVICES, AND THEIR SPECIFICITIES

Parameter	Unit of measurement	Measurement device	Measuring principle	Measurement range		Reported error
				Minimum	Maximum	
Turbidity	NTU	Lovibond TB211 IR	Nephelometric (90° scattered infrared light)	0.01 NTU	1100 NTU	±2.5% of reading, or ±0.01 NTU in the range of 0.01—500 NTU; ±5% of reading in the range of 500—1000 NTU
Turbidity	Volt	Setup A: DFRobot SEN0189 Setup B: Thermometrics TSW-10	Light attenuation (180° transmitted infrared light)	0 V	4.5 V	Unknown
Temperature	°C	Hanna Instruments HI98127 (pHep4)		−5.0 °C	60 °C	± 0.5 °C

wind and currents introduced uncertainty in the center sampling location within a radius of up to approximately 3 m.

Turbidity and temperature were measured for each of the locations in each reservoir (see Table III). The devices comprised a portable laboratory standard turbidimeter that was calibrated daily. The turbidimeter uses the nephelometric method, which measures the scattering of infrared light in the water, where the receptor is located at 90° from the light source [59]. Of the low-cost turbidity sensors, three pieces of two different manufacturers were bundled into two setups and connected to an Arduino microcontroller. The sensors emit infrared light and measure light attenuation in the water, where the receptor is located at 180° from the light source, in the form of an analog signal, which is translated into incoming voltage. The SEN0189 by DFRobot [60] is the most frequently used low-cost turbidity sensor in the scientific literature [40] and was used in Setup A. The Thermometrics TSW-10 in Setup B is a low-cost sensor that is used in household appliances [61]. The sensors were ordered at a price range of 10 € (SEN0189) to 26 € (TSW-10). Both sensor types were interfaced with a board delivered along with the sensor and connected to an LCD display to allow for quick verification of the data in the field. Data were recorded onto an SD card at 1 to 2-s intervals. A 3-D-printed casing for each of the sensor bundles, reinforced with black duct tape and sealed with silicone, stabilized the sensor heads and protected them from sunlight. Fig. 4 shows one of the sensor setups and water samples.

The two low-cost setups were both left in the sample to collect at least 30 readings. Layers of black duct tape shielded the samples in the polyethylene containers from ambient light. Rinsing with clean water after each sampling and washing the containers out with reservoir water before the next sampling avoided cross contamination. Turbidity with the professional turbidimeter and temperature were determined in triplicate and averaged. Temperature was taken with pH pens with integrated thermometers immediately at the sampling locations, whereas turbidity was measured at the bank.

2) In Situ Measurement Processing and Sensor Calibration: For the professional turbidimeter measurement, descriptive statistics were retrieved. For the low-cost sensor setups, the first three and last three measurements per sample were discarded from the series to exclude irregularities. We assessed the reliability of the low-cost sensors by calculating variances per turbidity range as measured with the turbidimeter and

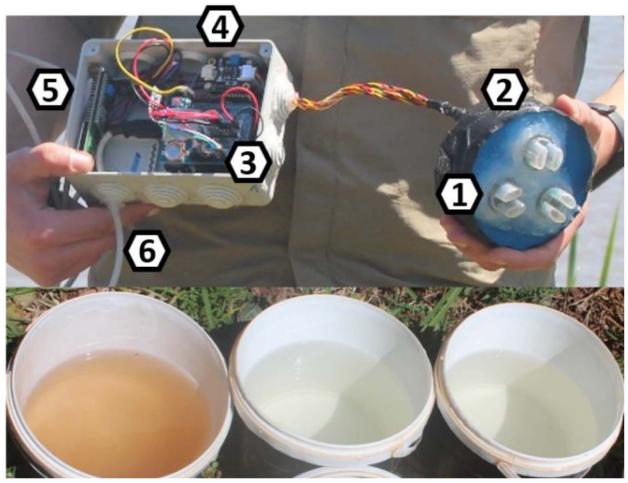

Fig. 4. (a) Sensor setup with (1) turbidity sensor heads, (2) 3-D-printed casing, (3) Arduino uno with additional board and SD card reader, (4) turbidity sensor board, (5) LCD display, and (6) power supply. (b) Samples from inflow, center, and outflow locations at 79, 6, and 7 nephelometric turbidity units (NTU) (left to right).

relative uncertainty defined as

$$\varepsilon = \frac{(V_i - \bar{V})}{\bar{V}} \tag{1}$$

where relative uncertainty equals the difference between each measured voltage reading V_i and average voltage per turbidity range $\bar{V}$ divided by the average voltage per turbidity range.

Subsequently, averages were calculated for each sensor per sample, as well as the overall averages across all sensors of each setup. Calibration models for the respective setup's averages were developed using the measurements in all locations ($n = 123$). We tested two calibration approaches. The first was a linear regression between the measured turbidity and voltage. For the second, we used multiple linear regression to account for water temperature. Temperature can impact electric transmission in turbidity sensors and it is generally recommended to correct for its influence, although it is not applied consistently [62], [63]. We measured calibration model performance with the coefficient of determination calculated as follows:

$$R^2 = 1 - \frac{SS_{\text{res}}}{SS_{\text{tot}}} \tag{2}$$

where SS_{res} is the sum of squared errors and SS_{tot} is the total sum of squares. The root-mean-squared error (RMSE) was calculated as

$$\text{RMSE} = \sqrt{\frac{\sum_{i=1}^{n} (y_i - \hat{y}_i)^2}{n}} \tag{3}$$

where n is the number of observations, y_i is the observed value at the observation i, and $\hat{y}_i$ is the value at the observation i as predicted by the model. The normalized RMSE (nRMSE) in percent scales the error by the value range and is calculated as

$$\text{nRMSE} = \frac{\text{RMSE}}{y_{\max} - y_{\min}} \times 100 \tag{4}$$

with $y_{\max}$ as the maximum and $y_{\min}$ as the minimum value. Bias is calculated as

$$\text{Bias} = \sum_{i=1}^{n} (\hat{y}_i - y_i). \tag{5}$$

After evaluation of variances, relative uncertainty, and calibration model performance metrics, the better-performing sensor setup was selected for further processing.

B. Remote-Sensing-Based Turbidity Modeling

1) C2RCC Preprocessing: In contrast to environments dominated by phytoplankton, such as the open ocean, which are referred to as Case-1 waters, Case-2 waters, such as inland water bodies, consist of relatively more inorganic substances, which makes them optically more complex [64]. The IOPs of Chl-*a*, TSM, and CDOM scatter and absorb light, and thus influence the reflectance of Case-2 waters [30], [65]. Inverting the radiative transfer model of incoming light allows to draw conclusions about the concentrations of these substances [65].

However, only between 2% and 10% of the reflected light yields information of the water column [66], [67]. Although it is possible to establish empirical relationships for the retrieval of optically active constituents, adequate water-specific atmospheric correction and bio-optical model-based IOP calculation allow for more robust subsequent retrieval of information on the organic and inorganic substances in the water [14], [54], [65].

The C2RCC processor inverts a comprehensive database of radiative transfer simulations using neural nets [30]. The semi-analytical bio-optical model is an expanded version of the Case 2 Regional algorithm by Doerffer and Schiller [29]. The model outputs six IOP components:

1) a_{pig}: pigment absorption related to chlorophyll;
2) a_{det}: absorption and scattering from detritus;
3) a_{gelb} for *gelbstoff*;
4) b_{wit} as a white scatterer;
5) b_{part} for typical sediment scattering;
6) b_{tot} for the sum of b_{part} and b_{wit} [16].

The C2RCC processor offers three sets of neural nets trained on a large database of remote sensing and in situ data for different scenarios: C2RCC for coastal applications, and C2X and C2X-COMPLEX (C2XC) for optically complex inland waters [16].

For this study, atmospheric correction with the C2RCC processor in ESAs Sentinel Applications Platform (SNAP) 9.0 was applied as it is based on physical understanding of optical water properties and has documented good performance [16], [53], [55], [68], also in small water bodies [69]. It is computationally efficient [70], [71] and its availability in SNAP along with Chl-*a* and TSM models renders it accessible to practitioners [16], [72], [73]. TSM is measured in mg/L and turbidity in nephelometric turbidity units (NTU), which refers to water clarity standards. Both turbidity and TSM are measures of particle load. Due to their close relationship [72], [74], we assume that matching the C2RCC TSM model can also be used to derive turbidity. The C2RCC TSM power model

$$\text{TSM} = \text{TSM}_{\text{fac}} * {b_{\text{tot}}}^{\text{TSM}_{\text{exp}}} \tag{6}$$

is based on the IOP b_{tot}. TSM_{fac} is a factor and TSM_{exp} is the exponent of the model. SNAP offers default values for the factor and the exponent, but adjustment with in situ data is recommended to achieve adequate results for a given scenario [16].

TABLE IV
C2RCC ATMOSPHERIC CORRECTION INPUT PARAMETERS FOR THE STUDY AREA AND PERIOD (01/2022–01/2023)

Parameter	Data	Value	Reference
Elevation (m a.s.l.)	SRTM	1766.5	[77]
Salinity (PSU)	-	0	-
Air pressure (hPa)	NCEP/NCAR Reanalysis	[1005—1012.6]	[78]
Temperature (°C)	NCEP/NCAR Reanalysis	[18.55—28.55]	[78]
Ozone (DU)	TOMS	[243—286]	[79]

C2RCC preprocessing accounts for elevation, salinity, air pressure, temperature, and ozone. We used the averaged elevation of the reservoirs from the shuttle radar topography mission (SRTM) digital elevation model and assumed salinity to be 0 practical salinity units (PSU). Air pressure and temperature were derived from the National Centers for Environmental Prediction (NCEP) and National Center for Atmospheric Research (NCAR) Reanalysis Project, and ozone concentration in Dobson Units (DU) from the total ozone mapping spectrometer (TOMS) product, all available in the Google Earth Engine catalog [75]. Out of the four available temperature and air pressure measurements per day, the 12:00 h corresponds best to the Sentinel-2 satellite overpass time at circa 10:30 h [76]. Temperature was converted from Kelvin to degrees Celsius (°C). Table IV displays the input parameter values and ranges.

This study covers the period from January 2022 to January 2023 (included), with all Sentinel-2 imagery <40% cloud cover at the 1C processing level downloaded from the Copernicus Open Access Hub.[1] After visual inspection, 34 images remained. Due to partial cloud cover over the reservoirs during the rainy seasons, more images had to be retained to achieve regular coverage of the reservoirs. All images were processed with the C2X and C2XC neural nets.

[1][Online]. Available: https://scihub.copernicus.eu

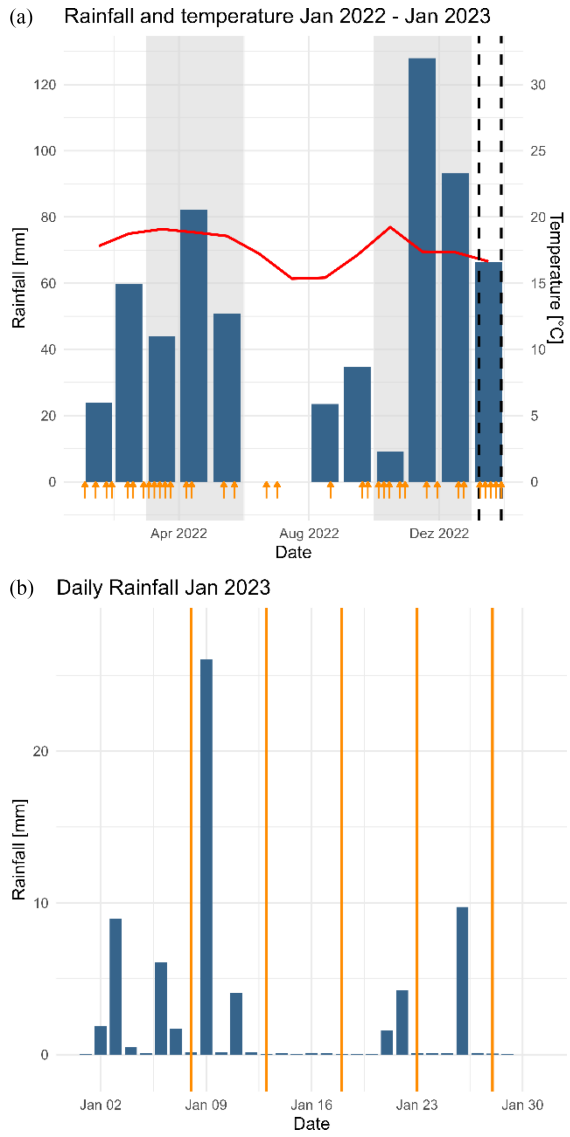

Fig. 5. (a) Rainfall and temperature measured at the Dedan Kimathi University of Technology campus, Nyeri, for January 2022–January 2023 with rainy seasons highlighted in gray, the sampling campaign indicated with black dashed lines, and the Sentinel-2 image dates with arrows. (b) Daily rainfall in January 2023, where lines indicate the Sentinel-2 overpasses.

2) Match-Up Generation of Sentinel-2 Imagery and In Situ Measurements: We generated match-ups of in situ turbidity measurements with the five Sentinel-2 overpasses in January 2023. The sampling campaign covered the end of the rainy season and the start of the dry season (see Fig. 5). The reservoirs showed considerable differences in turbidity. In combination with different rainfall patterns during the sampling campaign, we assumed that the samples reflect the local turbidity scenarios sufficiently well to calibrate the C2RCC turbidity models.

The five Sentinel-2 scenes were atmospherically corrected with C2RCC, which includes a pixel rejection algorithm for cloud. After visual inspection, the algorithm was adjusted to a slightly more generous inclusion of pixels for the 23rd of January, which was a higher cloud-cover day. Nevertheless, five of the ten reservoirs on that day were excluded. The output IOP values for both C2X and C2XC neural nets at the reservoirs' GPS-determined center locations were extracted within a 3×3 pixel window [16], [80] and averaged to reduce noise [70]. The sum of the IOPs b_{part} and b_{wit} returned b_{tot}, which is needed to calculate turbidity. The turbidimeter and low-cost sensor turbidity measurements were then matched with the b_{tot} values, resulting in 45 match-ups. We compared the turbidity models based on C2X and C2XC to determine the better-performing option using R^2, RMSE, and nRMSE. In addition, adjusted R^2 was calculated to assess model performance, which is robust in situations with skewed value distributions [81]. It is defined as

$$\text{Adjusted } R^2 = 1 - \frac{(1 - R^2) \times (n - 1)}{n - k - 1} \tag{7}$$

where R^2 is the coefficient of determination, n the number of observations, and k the number of predictor variables in the model. The remote-sensing models fitted with low-cost measurements were additionally validated against the turbidimeter measurement to get independent accuracy metrics.

TABLE V
MEAN, MEDIAN, STANDARD DEVIATION, AND RANGE OF TURBIDITY MEASUREMENTS IN NTU FOR THE INFLOW, CENTER, AND OUTFLOW LOCATIONS

Statistic	Turbidity (NTU)		
	Inflow (n = 35)	Center (n = 50)	Outflow (n = 38)
Mean	39.26	31.32	23.83
Median	16.60	13.44	13.84
Standard deviation	46.70	41.32	23.41
Range	[7.60—226.0]	[5.18—145.0]	[5.52—108]

IV. RESULTS

A. In Situ Water Quality Measurements

Table V presents summary statistics of inflow, center, and outflow turbidity measurements. Turbidity is generally higher at the inflow compared with center and outflow locations and the standard deviation and value range is larger. Mean outflow turbidity is almost eight NTU below center turbidity. However, the median values of outflow and center measurements are comparable. A complete table with all measured values is in the Annex.

The Kenya Bureau of Standards (KEBS) defines the acceptable turbidity limit for natural potable water below 25 NTU [82]. Six out of the ten reservoirs exceeded the KEBS-defined turbidity limit at least once at least in one sampling location. Kiunyu, Ndaruku, Karia, and Njeng'u Dams had turbidity levels over 25 NTU at their inflow or at their outflow locations, while the reservoir water body remained below the limit. Samaki and Kagati Dam exceeded the KEBS limit throughout the sampling period in all sampling locations. For all locations, 28% of sampled turbidity values were above 25 NTU and for center locations, 20% exceeded the threshold.

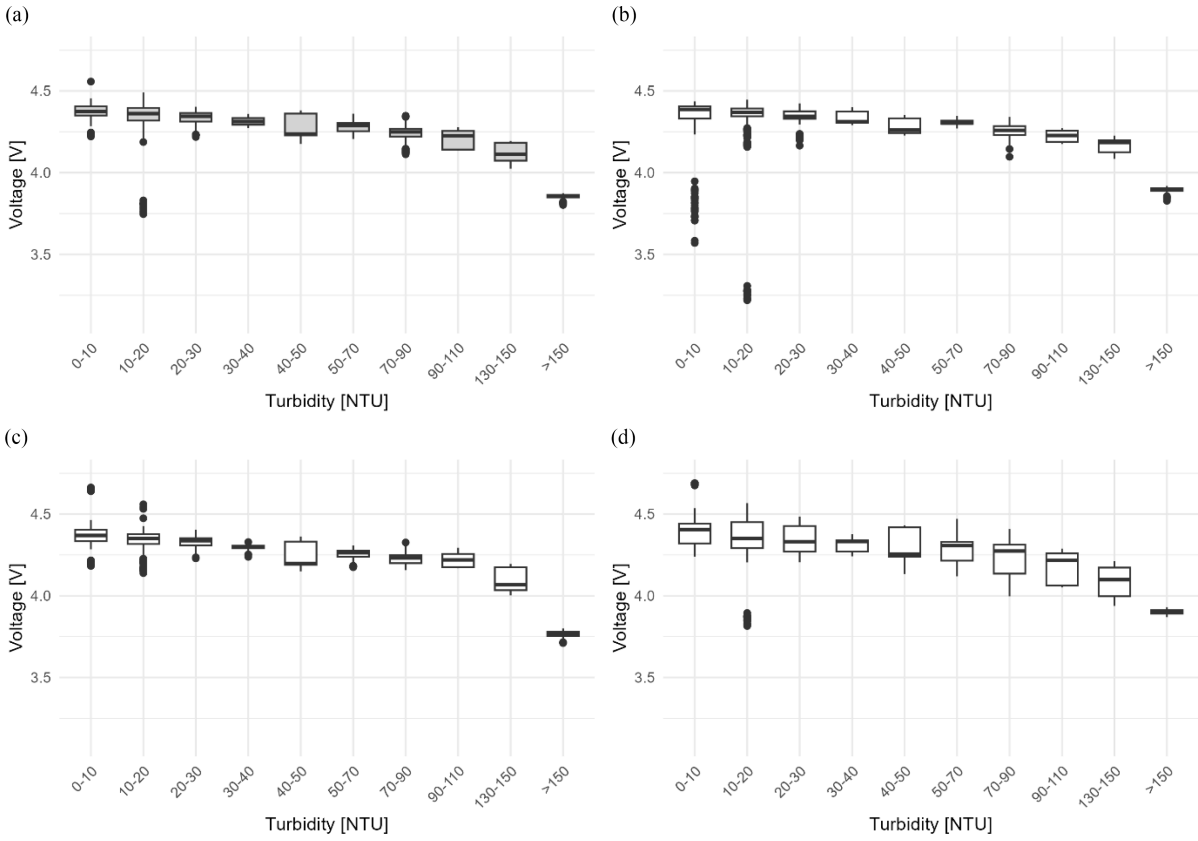

Fig. 6. Setup A: Measured voltage in [V] within turbidimeter-measured turbidity in [NTU] for (a) mean of all three sensors and (b)–(d) individual sensor measurements. (a) Setup A vs. measured NTU. (b) Setup A.1 vs. measured NTU. (c) Setup A.2 vs. measured NTU. (d) Setup A.3 vs. measured NTU.

B. Low-Cost Sensor Selection and Calibration

Sensor uncertainty shows how stable the measurements are. Figs. 6 and 7 show the averaged and individual sensor values per turbidimeter-measured turbidity range for Setup A (SEN0189) and Setup B (TSW-10). Setup A had reasonably stable values across the value ranges that occurred in the studied reservoirs. Outliers occurred mostly in lower turbidity ranges between 0 and 30 NTU. Although outliers in these ranges remained, with the most obvious ones between 10 and 20 NTU, averaging across the sensors improved the result. In contrast, all of the Setup B sensors were measured with low precision and high variance across all turbidity value ranges. Averaging did not lead to a robust result with a distinct pattern.

Fig. 8 shows the relative uncertainty of values averaged across the three sensors per setup against turbidimeter measurements. The relative uncertainties per NTU value range stay narrow for the averaged Setup A measurements, except for outliers in the 10–20 NTU range. Setup B has overall higher relative uncertainty across all turbidity ranges and various positive and negative outliers. Due to the considerably better performance of Setup A, we selected this setup for further analysis. We used the averaged value from the three single sensors to increase robustness.

Raw values are usually converted to turbidity in a calibration step to obtain a physically meaningful parameter, where passing voltage is inversely proportional to turbidity [40], [60]. To be able to relate the subsequent remote-sensing models to the same physical parameter and ensure comparability, a calibration model was set up to convert the averaged passing voltage measurements from Setup A to turbidity in NTU. Negative predictions were considered as 0 NTU.

TABLE VI
SETUP A CALIBRATION MODEL METRICS USING ALL INPUT DATA, EXCLUDING ONE OUTLIER, AND WITH COMPENSATING FOR TEMPERATURE DIFFERENCES

Calibration Model	r	R^2	RMSE (NTU)	nRMSE (%)	Bias
All data	0.73	0.53	26.4	16.9	0.13
After outlier exclusion	0.85	0.71	20.2	14.4	0.74
With temperature compensation	0.86	0.73	19.7	14.1	0.70

Table VI presents the accuracy metrics of the linear conversion models. When all data points are used, $R^2 = 0.53$. We then excluded one outlier that was likely due to the sampling bucket not being filled with enough water, which strongly improved the accuracy metrics. Compensating for temperature further improved all metrics. However, the improvement is so slight that temperature may be neglected in this scenario, which yields the advantage of not relying on an additional parameter.

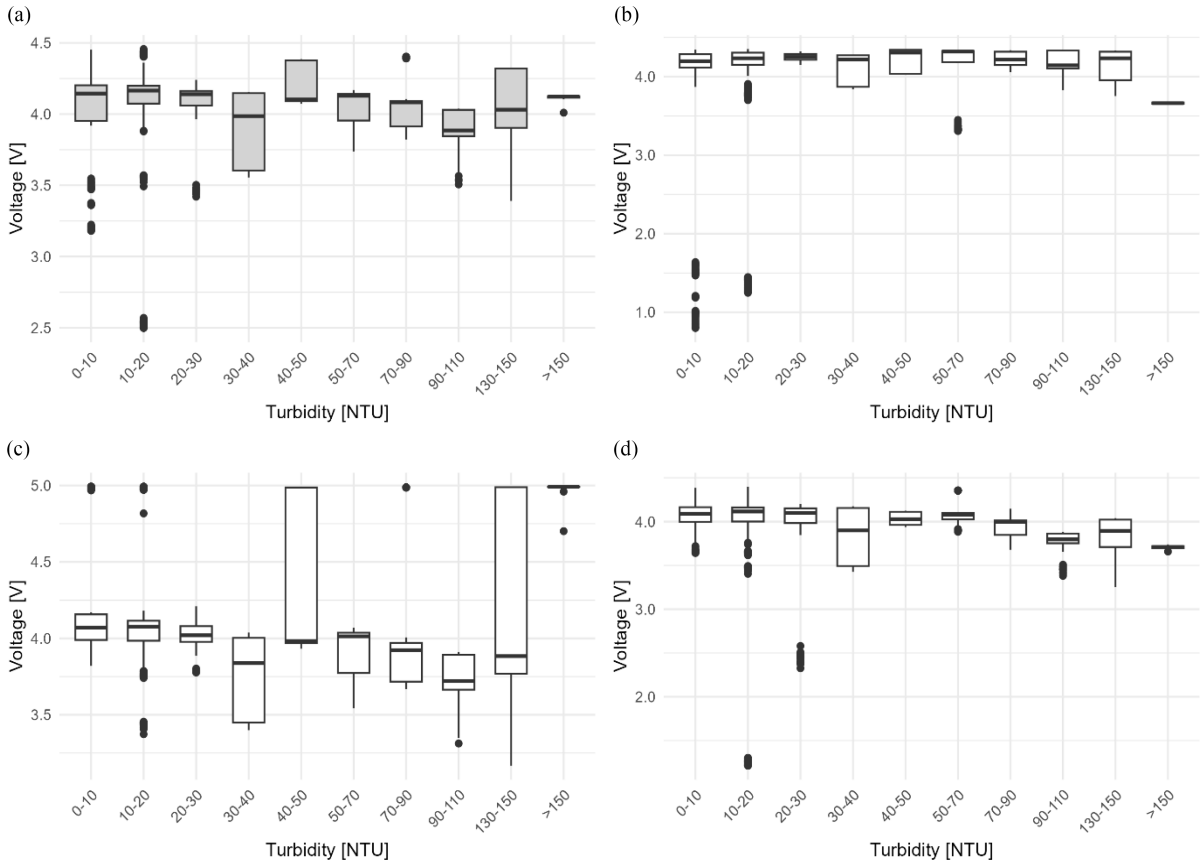

Fig. 7. Setup B: Measured voltage in [V] within turbidimeter-measured turbidity in [NTU] for (a) mean of all three sensors and (b)–(d) individual sensor measurements. (a) Setup B vs. measured NTU. (b) Setup B.1 vs. measured NTU. (c) Setup B.2 vs. measured NTU. (d) Setup B.3 vs. measured NTU.

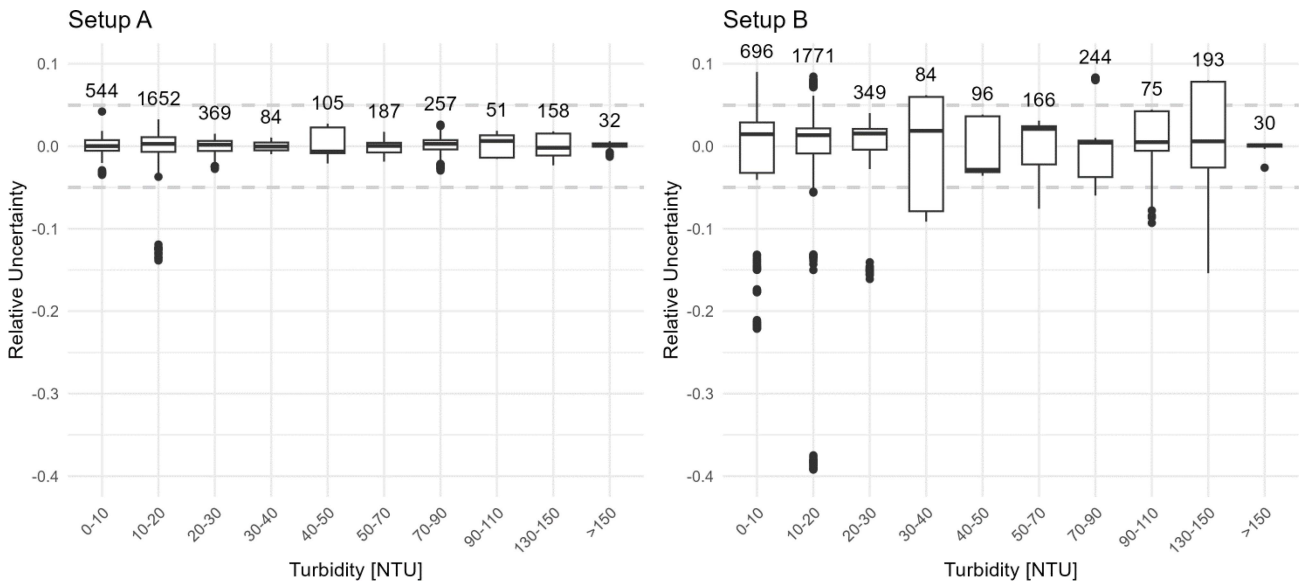

Fig. 8. Relative uncertainties of all Setup A and Setup B voltage measurements within turbidimeter-measured NTU measurement ranges, including the number of measured instances per bin. The dashed line indicates ±5%.

TABLE VII
ACCURACY METRICS OF THE C2X AND C2XC TURBIDITY MODELS FITTED WITH TURBIDIMETER AND LOW-COST SENSOR MEASUREMENTS

Turbidity model	Parameterization	Accuracy metrics	R^2	Adjusted R^2	RMSE (NTU)	nRMSE (%)
C2X	Turbidimeter measurements	Inherent	0.63	0.52	26.8	19.2
C2X	Low-cost measurements	Inherent	0.65	0.64	23.4	16.7
		Against turbidimeter measurements	0.45	0.44	29.1	20.8
C2XC	Turbidimeter measurements	Inherent	0.83	0.72	20.5	14.7
C2XC	Low-cost measurements	Inherent	0.76	0.75	19.5	13.9
		Against turbidimeter measurements	0.62	0.61	24.3	17.4

C. Turbidity Model Performance and Results

Table VII provides an overview of the turbidity models using C2X and C2XC each fitted with turbidimeter measurements and with low-cost sensor measurements. The performances of the C2X models have higher RMSE and nRMSE, and lower R^2 and adjusted R^2. The C2XC model fitted with the low-cost measurements has lower RMSE and nRMSE than the other C2XC model, but also a lower R^2. With 0.75, its adjusted R^2 is slightly superior to that of the C2XC model fitted with turbidimeter measurements ($R^2 = 0.72$). However, when tested against the turbidimeter measurements, the C2XC model fitted with low-cost data decreases its accuracy. The accuracy metrics are inferior to the inherent accuracy metrics of the C2X model fitted with low-cost measurements, but again superior when the C2X model predictions are compared with the turbidimeter measurements. Even when fitted with low-cost measurements, the C2XC model is still more accurate than the C2X model fitted with turbidimeter measurements.

The scatterplots in Fig. 9 show the C2X and C2XC models fitted with turbidimeter and with low-cost measurements. For all models, most of the input values are at the lower NTU and b_{tot} range, which is reflected in the lower adjusted R^2. Most of the variability is found from 50 NTU upward but is lower for C2XC. The C2XC models have a steeper curve that leads to more accurate estimation of higher turbidity, whereas the C2X models underestimate high ranges more strongly. Both low-cost measurement fitted models show clearer overestimation of low NTU ranges and underestimation of higher NTU ranges. The predictions of the C2X and the C2XC model pair each cross the 25 NTU threshold closely to each other.

A time series for all reservoirs from January 2022 to January 2023 is derived from the C2XC turbidity model using turbidimeter measurements and the C2XC model using low-cost measurements (see Fig. 10). Overestimation in low-turbidity ranges and underestimation in high-turbidity ranges for the low-cost model reproduce in the time series. However, both models' estimations lie closely to each other and reflect distinct turbidity regimes. According to the time series, the reservoirs can be clustered into three groups. Ithenguri, Kiunyu, Ndaruku, Karia, Njeng'u, and Ruthagati reservoirs remain below the critical threshold of 25 NTU almost throughout the whole year. Turbidity peaks above the threshold happen around the short rainy season for Ithenguri, Kiunyu, Karia, and Ruthagati, whereas in the case of Kiunyu, fluctuations around the threshold occur throughout the year. Hombe and Hohwe constitute the second group with strong turbidity peaks during both wet seasons, but turbidity levels below 25 NTU during the dry season from June to August 2022. Samaki and Kagati are characterized by high-turbidity levels during most of the year. In general, the low-cost sensor-based model tends to estimate an earlier rise of turbidity past the turbidity threshold and a later descent below it.

V. DISCUSSION

In this study, we tested the potential of using low-cost turbidity measurements and a remote-sensing model together to monitor water quality in a wetland landscape in Kenya. We identified and calibrated the better-performing sensor setup. We used these measurements and turbidimeter measurements to parameterize the C2RCC bio-optical model and successfully applied two versions in the context of Kenyan surface water monitoring guidelines. These results have implications regarding the suitability of turbidity modeling in small reservoirs and the suitability of low-cost turbidity measurements for monitoring and modeling water quality. Furthermore, we discuss the implications of the measured and modeled results for wetland agroecosystems, and how the tools can be applied to an operational turbidity monitoring context while improving community engagement.

A. Suitability of the Remote-Sensing-Based Approach to Model Small Reservoir Turbidity

Small inland water bodies pose several challenges to remote-sensing approaches, where optically active constituents create unique patterns of interactions that are difficult to disentangle and may be enhanced by the presence and seasonality of aquatic vegetation [83], [84]. Banks or vegetation that are located near the water surface lead to atmospheric scattering above the water and cause adjacency effects [85], [86]. Due to the comparable and small reservoir sizes, we assumed adjacency effects to be approximately similar across sites. We also assumed comparable sediment color and type based on the prevalent deep clayey soils, c.f., [87]. Different assemblages of semiaquatic and aquatic vegetation were generally present at all sites. However, they mostly occurred close to the banks. As the match-ups were generated from center locations, their influence on the resulting models is likely to be small. However, when applying the models

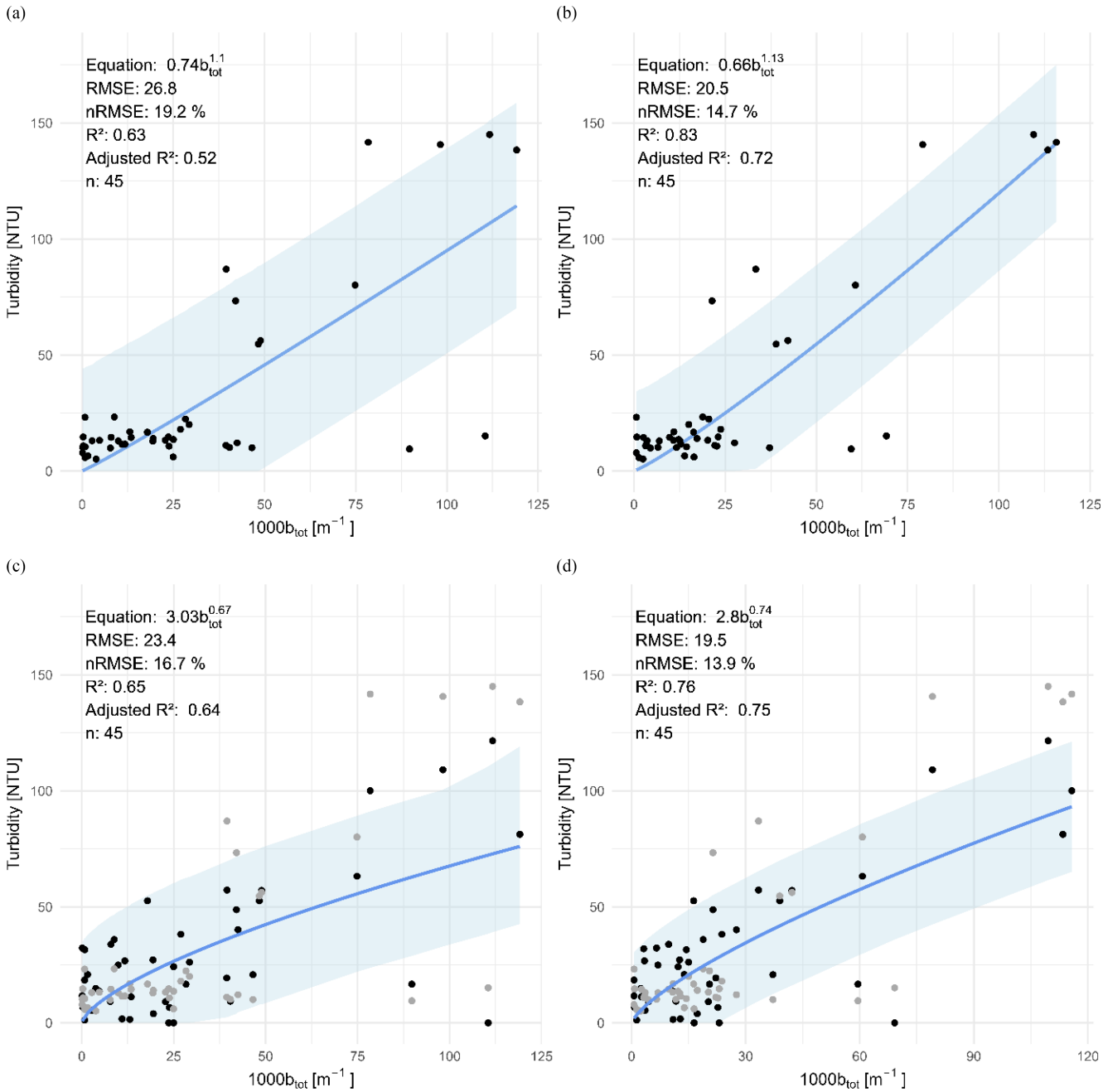

Fig. 9. Turbidity models using A C2X and B C2XC neural nets and center location turbidimeter measurements, and using C C2X and D C2CX neural nets with turbidity calculated by conversion of voltage from Setup A. For C and D, the turbidimeter-measured values from A and B are superimposed in gray. Light blue shading indicates the 95% confidence level. (a) C2X. (b) C2XC. (c) C2X Low-cost. (d) C2Xc Low-cost.

on the surface, it must be taken into account that plants can impact the result in these areas and may need to be excluded, if they are not automatically rejected through the C2RCC water mask. Fig. 11 shows modeled turbidity in Hohwe Dam for a dry- and a rainy-season image. For both images, the turbidity of the border pixels differs visibly from the major part of the reservoir, which may be attributable to vegetation and other effects near the bank.

Despite these simplifications, our results show that the parameterized C2RCC models are generally useful in determining turbidity in small reservoirs with both C2XC neural nets based model parameterizations performing better than the C2X ones. The C2XC model we fitted with low-cost sensor measurements has a lower R^2 of 0.62 compared with its turbidimeter measurement fitted counterpart with an R^2 of 0.83. However, all metrics compared, it still performs better than the turbidimeter-fitted C2X model. The time series of the C2XC models shows good agreement between them in reproducing distinct turbidity regimes across the year. The lower sensitivity of the low-cost sensors at low and the quicker saturation at high-turbidity ranges compared with the turbidimeter translate into an overestimation of low values and an underestimation of high values in the

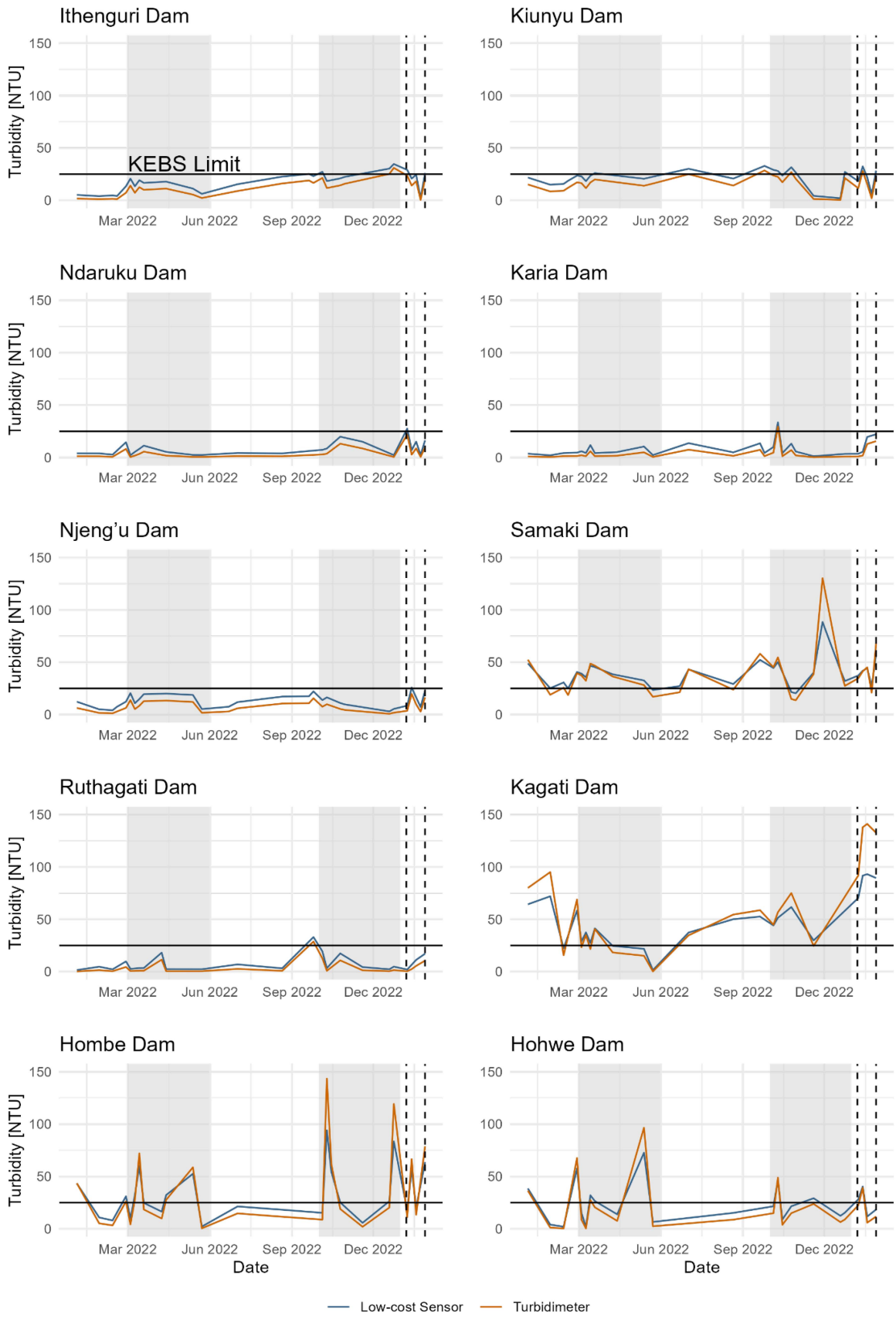

Fig. 10. Time series of turbidity as modeled with the C2XC neural nets from converted low-cost measurements (blue) and turbidimeter measurements (orange) from January 2021 to January 2023. Dashed lines indicate the time of the sampling campaign; the horizontal line is the KEBS limit for natural potable water of 25 NTU.

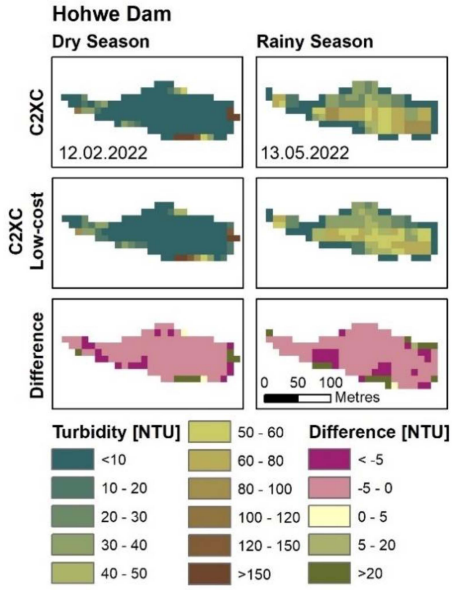

Fig. 11. Turbidity modeled for Hohwe dam for a dry-season Sentinel-2 image (12.02.2022) and for a rainy-season image (13.05.2022) using the C2XC model calibrated with turbidimeter measurements and the C2XC model calibrated with low-cost measurements, as well as difference images of the latter subtracted from the former.

time series. We did not apply other semianalytical or empirical turbidity models to evaluate if these perform better in the low or high-turbidity ranges. Nevertheless, the developed models agree well in particular at the intermediate turbidity range that is of interest in the Kenyan context.

Our model accuracy metrics are in the intermediate to high ranges relative to previous publications. Several studies report good results using C2RCC with different neural nets for river, lake, and coastal environments in intermediate turbidity ranges, where some applied their own band calculations, e.g., [88] and [89], and some also used the IOP-based model, e.g., [16], [70], and [72]. Where different neural nets or different environments were compared, these had a strong impact on the model performance and results. Lock et al. [72], therefore, emphasize that the knowledge of the ecosystem is necessary to understand under which scenario the respective remote-sensing-based turbidity retrieval works. Our study confirms the necessity to validate C2RCC models for individual environments. It also shows that choosing the neural nets that fit this environment is critical to achieve good results. Low-cost measurements can potentially be used to guide neural nets selection, and for model parameterization, where professional equipment is unavailable, although their precision is limited in very low and very high-turbidity ranges. For our purpose, the turbidity limit of concern at 25 NTU was sufficiently well resolved. Although the models fitted with low-cost measurements performed less well in terms of retrieving absolute values, the difference in accuracy metrics between the low-cost models is reproduced in the turbidimeter-fitted models. Therefore, low-cost measurements can also be useful for relative comparison between different turbidity models in a specific environment, or in the case of C2RCC, for relative comparison between neural nets.

B. Suitability of Low-Cost Turbidity Sensors to Assess Small Reservoir Turbidity

The popularity of low-cost sensor technology is steadily increasing as an accessible alternative to conventionally used equipment. Yet, studies often focus on setting up a functional system, where only a fraction calibrate their equipment and report accuracy metrics [40]. Our results from 123 samples taken with two different sensor types demonstrate how sensors with similar technical specifications can measure completely different values. Due to high variability and outlier occurrence, we discarded one sensor setup and averaged values across the other to increase robustness. Calibration of the averaged values resulted in an R^2 of 0.53, 0.71, and 0.73 for all measurements, excluding an outlier, and for multiple regression with temperature compensation. Turbidity measurements below 20 NTU generally showed higher uncertainty.

Our low-cost sensor calibration model is less accurate than those of several studies on low-cost sensors that compared their measurements with those of turbidimeters. They often report R^2 for the SEN0189 or similar sensors that are close to 1, e.g., [90] and [91]. However, these results are achieved in controlled environments. Droujko and Molnar [92] found that their Formazin standard-calibrated sensors did not perform well with the sediments dominating the studied river network and, therefore, suggested to bypass laboratory sensor calibration altogether. Accordingly, our higher calibration error under real-life conditions may be a better indicator of how operational sensor measurements are subjected to local environmental parameters, particle size and type, and interaction with other water constituents. This means sensors need specific local instead of standardized calibration. Measuring mistakes can have big impacts on the calibration algorithm. At the same time, temperature may be neglected in similar scenarios. Sensor assessment through variability and uncertainty analysis helps to determine suitable sensor candidates, and clustering increases robustness, c.f. [93].

The differences in uncertainty across turbidity value ranges may be attributable to mixed effects, including different sensor sensitivities in the turbidity ranges, uneven distribution of the numbers of samplings, or the concentration of other optically active constituents, such as algae. Low performance in low-turbidity ranges, as reported by Gillett and Marchiori [90], limits the potential of low-cost sensors for low-turbidity uses, such as drinking water assessment. However, accuracies in our target value range were sufficient.

C. Implications of Turbidity on Wetland and Water Management

Turbidity has implications for irrigation, livestock, and aquaculture. High turbidity can lead to the clogging of irrigation systems and high sediment load can incite yield penalties [94]. High particle load leads to siltation of reservoirs [13]. High turbidity in silted reservoirs can also increase the occurrence

of livestock diseases [2] and negatively impact fish populations [94]. The turbidity levels we measured and modeled between January 2022 and January 2023 differed strongly. Four reservoirs remained within the Kenyan limits for natural potable water of below 25 NTU [82] for most of the time. Two reservoirs had strong peaks above the threshold during the wet seasons, and two reservoirs exceeded the threshold for most of the time. This may affect water and wetland use to some extent at several sites either temporally or permanently during the year. The turbidity levels are consistent with published results of surface water samplings in tropical environments, e.g., [95], [96], and [97]. Seasonality and land management practices impact turbidity [98], [99], [100] and could be factors in the context of the studied reservoirs.

D. Operational Monitoring and Community Engagement

Water resources in multifunctional agroecosystems require observation to quantify interlinkages and improve management practices [101]. Remote sensing and low-cost sensor technology are increasingly applied for this purpose and come with inherent opportunities and challenges. Optical satellite remote-sensing methods to retrieve turbidity suffer from missing observations through cloud cover [102] and authors report varying results in turbidity model accuracy for different water body types and environments [16], [70], [72]. Low-cost Internet of Things and citizen science approaches to environmental monitoring tie the meshes of measuring nets tighter [103]. Low-cost sensors are often easy to use [104], but also easy to break [40]. In the case of Corbari et al. [36], out of 456 deployed low-cost sensor stations, 69 were not operational, and many only provided data for a few days. Pitfalls to the implementation of low-cost water quality measurement schemes are sensor degradation, vandalism, and nonuse by the water user communities [42].

In this study, we experienced most of the common issues that affect both of these technologies. Even so, we could parameterize, validate, apply, and compare models to gain insights into the reservoirs' turbidity regimes with low resource usage. The turbidity time series is a starting point to quantify the impact of relevant factors in the wetland context, including surface water dynamics, land cover, information on wetland species and disturbances, or wetland use intensity [105], [106], [107], [108], [109], [110], [111], [112], [113]. Some authors have removed small wetland reservoirs from their assessment frameworks [114]. Yet, as surface water bodies, they serve as a window to wetland water quality. Low-cost water quality sensors can help to calibrate and validate remote-sensing algorithms and to complement missing imagery. Proper merging of the information from dense sensor networks with remote sensing could help to improve water resources management and agricultural monitoring activities, overcoming the problems of each type of data [36].

Integrating measurements in—for example—the local citizen science tool for environmental monitoring by Kipkemboi et al. [50] could serve as a foundation for community engagement, sensitization, and streamlining data collection. Moreover, water serves as an effective vehicle for concepts in science, technology, engineering, and mathematics subjects [115] and geospatial secondary [116], [117] and tertiary education [118]. The implementation of a user-driven community of practice could lead to further improvement of spatial planning processes and increase technical skills.

VI. Conclusion

This study assessed a remote sensing and low-cost turbidity sensor-based approach to model turbidity in ten small wetland reservoirs in Nyeri, Kenya. Turbidity is a water quality parameter in itself and can also be used as an indicator of overall water quality. Highly performant bio-optical water quality models, such as the C2RCC processor, have the potential to fill ground monitoring gaps. However, mixed results in the literature show the need for ground validation, where small inland water bodies are particularly challenging due to complex interactions of optically active water constituents and atmospheric scattering effects.

Low-cost water quality sensors provide a possible inexpensive alternative where professional equipment is not available for continuous field measurements or is not a resource-efficient option. In situ measurements showed reasonable or good performance. They proved to be capable of checking the suitability of the C2RCC processor for the study site, to select the better-performing neural nets, and to parameterize the models based on the resulting IOP. Despite inaccuracies introduced through the low-cost measurements, both C2XC models were in strong agreement in terms of the reservoir turbidity regimes. Where laboratory equipment is not or not often available, low-cost measurements can support monitoring and provide other benefits, such as increased community engagement, environmental sensitization, and technical capacity building.

Existing models can be applied for operational turbidity monitoring in small wetland reservoirs. Using remote sensing and low-cost in situ measurements together increases the data basis and flexibility of the approach with respect to the advantages and disadvantages of both technologies for continuous water turbidity monitoring. It could be a good option to close data gaps, enhance the involvement of the local community, improve management, and reduce risks around food and water use from dammed wetlands.

Author Contributions

Stefanie Steinbach: Conceptualization, Methodology, Investigation, Formal analysis, Visualization, Writing – Original draft, Writing – Review and Editing. Martin W. Chege: Investigation, Writing – Review and Editing. Niels Dedring: Investigation, Writing – Review and Editing. Wisdom Kipkemboi: Investigation, Writing – Review and Editing Andreas Rienow: Investigation, Resources, Supervision, Writing – Review and Editing. Bartholomew Thiong'o Kuria: Investigation, Writing – Review and Editing. Sander Jaap Zwart: Conceptualization, Methodology, Supervision, Writing – Review and Editing. Andrew Nelson: Conceptualization, Methodology, Supervision, Writing – Review and Editing.

TABLE VIII
TURBIDITY VALUES MEASURED IN TEN SMALL RESERVOIRS IN NYERI COUNTY, KENYA

Reservoir	Location	Turbidity (NTU)				
		07/01/2023–08/01/2023	13/01/2023–14/01/2023	18/01/2023–19/01/2023	23/01/2023–24/01/2023	27/01/2023-28/01/2023
Ithenguri Dam	Inflow	13.73	16.6	23.77	13.07	22.87
	Center	17.97	20.03	23.3	23.17	22.4
	Outflow					
Kiunyu Dam	Inflow					
	Center	12.9	12.13	16.73	14.47	14.7
	Outflow	18.07	16.67	**25.1**	13.6	
Ndaruku Dam	Inflow	9.89	7.6	10.22	**33.6**	10.97
	Center	11.07	11.6	14.53	14.67	16.9
	Outflow	14.07	15.8	20.73	20.43	**54.23**
Karia Dam	Inflow	**57.1**	**88.3**	**86.87**	**95.9**	**79.43**
	Center	5.82	5.18	6.54	5.71	6.06
	Outflow	5.52	5.87	6.02	5.65	7.31
Njeng'u Dam	Inflow	9.55	**29.67**	22.7	18.7	**25.13**
	Center	9.91	13.27	13.23	13.07	14.03
	Outflow	13	11	11.53	12.03	11.47
Samaki Dam	Inflow	**226**	**144.67**	**89.43**	**68.23**	**45.1**
	Center	**86.97**	**54.7**	**56.23**	**73.33**	**80.1**
	Outflow	**48.33**	**61.7**	**108**	**81.2**	**71**
Ruthagati Dam	Inflow	8.38	11.16	15.17	13.73	12.8
	Center	7.85	10.84	10.2	9.91	10.14
	Outflow	7.6	10.73	9.49	9.25	10.4
Kagati Dam	Inflow					
	Center	**140.67**	**138.33**	**141.67**	**141.33**	**145**
	Outflow		**27.9**	**40.47**	**30.43**	**33.07**
Hombe Dam	Inflow	12.6	12.2	10.92	12.6	15.27
	Center	13.6	9.51	10.44	13.6	15.13
	Outflow	11.73	19.17	9.83	11.73	15.27
Hohwe Dam	Inflow					
	Center	10.73	10.04	12.97	12	11.53
	Outflow					

Measurements exceeding the limits set by the KEBS are marked in bold.

APPENDIX

See Table VIII.

ACKNOWLEDGMENT

The authors would like to thank J. Wanjala for her engagement in the prestudies, S. Muthee, A. Bartels, and M. Goebel who supported the planning and realization of the January 2023 field study, as well as Dr. F. Kirimi for her short-term involvement; our committed drivers S. Kinyanjui and M. Waithaka without whom the implementation of the campaign would not have been possible; and Dr. F. Binz, T. Dedring, J. de Vos, R. Hiby, Dr. C. Kyba, J.-P. Langenkamp, I. Tertel, and P. Podkowa, Dr. J. Schultz, Dr. D. van der Wal, M. Wieczorek, and the RUB GI laboratory staff for discussions and advice on specific aspects of data collection and analysis. Planet data for study site visualization has been provided under the NICFI Satellite Data Program. Access to the part of the upper Tana basin and collection of required data was kindly facilitated by the Muringato Water Resource Users Association (WRUA).

REFERENCES

[1] A. Ogilvie, G. Belaud, S. Massuel, M. Mulligan, P. L. Goulven, and R. Calvez, "Assessing floods and droughts in ungauged small reservoirs with long-term Landsat imagery," *Geosciences*, vol. 6, no. 4, Sep. 2016, Art. no. 42, doi: 10.3390/geosciences6040042.

[2] D. Saruchera and J. Lautze, "Small reservoirs in Africa: A review and synthesis to strengthen future investment," International Water Management Institute, Accra, Ghana, 2019, doi: 10.5337/2019.209.

[3] S. Kibret, M. McCartney, J. Lautze, L. Nhamo, and G. Yan, "The impact of large and small dams on malaria transmission in four basins in Africa," *Sci. Rep.*, vol. 11, no. 1, Jun. 2021, Art. no. 13355, doi: 10.1038/s41598-021-92924-3.

[4] B. Ghansah, T. Foster, T. P. Higginbottom, R. Adhikari, and S. J. Zwart, "Monitoring spatial-temporal variations of surface areas of small reservoirs in Ghana's upper east region using Sentinel-2 satellite imagery and machine learning," *Phys. Chem. Earth, Parts A/B/C*, vol. 125, Feb. 2022, Art. no. 103082, doi: 10.1016/j.pce.2021.103082.

[5] B. Mati, "Farmer-led irrigation development in Kenya: Characteristics and opportunities," *Agricultural Water Manage.*, vol. 277, Mar. 2023, Art. no. 108105, doi: 10.1016/j.agwat.2022.108105.

[6] P. Woodhouse, G. J. Veldwisch, J.-P. Venot, D. Brockington, H. Komakech, and Â. Manjichi, "African farmer-led irrigation development: Re-framing agricultural policy and investment?," *J. Peasant Stud.*, vol. 44, no. 1, pp. 213–233, Jan. 2017, doi: 10.1080/03066150.2016.1219719.

[7] B. Bahilu and M. Tadesse, "Review on distribution, importance, threats and consequences of wetland degradation in Ethiopia," *Int. J. Water Resour. Environ. Eng.*, vol. 9, no. 3, pp. 64–71, Mar. 2017, doi: 10.5897/IJWREE2016.0697.

[8] P. Nakawuka, S. Langan, P. Schmitter, and J. Barron, "A review of trends, constraints and opportunities of smallholder irrigation in East Africa," *Glob. Food Secur.*, vol. 17, pp. 196–212, Jun. 2018, doi: 10.1016/j.gfs.2017.10.003.

[9] A. Uwimana, A. van Dam, G. Gettel, B. Bigirimana, and K. Irvine, "Effects of river discharge and land use and land cover (LULC) on water quality dynamics in Migina catchment, Rwanda," *Environ. Manage.*, vol. 60, no. 3, pp. 496–512, Sep. 2017, doi: 10.1007/s00267-017-0891-7.

[10] T. Abiye, "The role of wetlands associated to urban micro-dams in pollution attenuation, Johannesburg, South Africa," *Wetlands*, vol. 35, no. 6, pp. 1127–1136, Dec. 2015, doi: 10.1007/s13157-015-0700-0.

[11] A. Uwimana, A. A. van Dam, and K. Irvine, "Effects of conversion of wetlands to rice and fish farming on water quality in valley bottoms of the Migina catchment, Southern Rwanda," *Ecol. Eng.*, vol. 125, pp. 76–86, Dec. 2018, doi: 10.1016/j.ecoleng.2018.10.019.

[12] N. De Troyer, S. Mereta, P. Goethals, and P. Boets, "Water quality assessment of streams and wetlands in a fast growing east African city," *Water*, vol. 8, no. 4, Mar. 2016, Art. no. 123, doi: 10.3390/w8040123.

[13] R. S. Winton, E. Calamita, and B. Wehrli, "Reviews and syntheses: Dams, water quality and tropical reservoir stratification," *Biogeosciences*, vol. 16, no. 8, pp. 1657–1671, Apr. 2019, doi: 10.5194/bg-16-1657-2019.

[14] K. Dörnhöfer and N. Oppelt, "Remote sensing for lake research and monitoring—Recent advances," *Ecol. Indicators*, vol. 64, pp. 105–122, May 2016, doi: 10.1016/j.ecolind.2015.12.009.

[15] P.-W. Su and S.-L. Lo, "Satellite imagery: A way to monitor water quality for the future?," *Environ. Sci. Pollut. Res.*, vol. 29, no. 38, pp. 57022–57029, Aug. 2022, doi: 10.1007/s11356-022-21524-z.

[16] J. Soriano-González et al., "Towards the combination of C2RCC processors for improving water quality retrieval in inland and coastal areas," *Remote Sens.*, vol. 14, no. 5, Feb. 2022, Art. no. 1124, doi: 10.3390/rs14051124.

[17] E. Spyrakos et al., "Optical types of inland and coastal waters," *Limnol. Oceanogr.*, vol. 63, no. 2, pp. 846–870, Mar. 2018, doi: 10.1002/lno.10674.

[18] I. Chawla, L. Karthikeyan, and A. K. Mishra, "A review of remote sensing applications for water security: Quantity, quality, and extremes," *J. Hydrol.*, vol. 585, Jun. 2020, Art. no. 124826, doi: 10.1016/j.jhydrol.2020.124826.

[19] M. W. Matthews, "A current review of empirical procedures of remote sensing in inland and near-coastal transitional waters," *Int. J. Remote Sens.*, vol. 32, no. 21, pp. 6855–6899, Nov. 2011, doi: 10.1080/01431161.2010.512947.

[20] J. C. Ritchie, P. V. Zimba, and J. H. Everitt, "Remote sensing techniques to assess water quality," *Photogramm. Eng. Remote Sens.*, vol. 69, no. 6, pp. 695–704, Jun. 2003, doi: 10.14358/PERS.69.6.695.

[21] V. Sagan et al., "Monitoring inland water quality using remote sensing: Potential and limitations of spectral indices, bio-optical simulations, machine learning, and cloud computing," *Earth Sci. Rev.*, vol. 205, Jun. 2020, Art. no. 103187, doi: 10.1016/j.earscirev.2020.103187.

[22] J. Sheffield et al., "Satellite remote sensing for water resources management: Potential for supporting sustainable development in data-poor regions," *Water Resour. Res.*, vol. 54, no. 12, pp. 9724–9758, Dec. 2018, doi: 10.1029/2017WR022437.

[23] M. K. Lehmann, E. M. Schütt, M. Hieronymi, J. Dare, and H. Krasemann, "Analysis of recurring patchiness in satellite-derived chlorophyll *a* to aid the selection of representative sites for lake water quality monitoring," *Int. J. Appl. Earth Observ. Geoinf.*, vol. 104, Dec. 2021, Art. no. 102547, doi: 10.1016/j.jag.2021.102547.

[24] K. Toming, T. Kutser, A. Laas, M. Sepp, B. Paavel, and T. Nõges, "First experiences in mapping lake water quality parameters with Sentinel-2 MSI imagery," *Remote Sens.*, vol. 8, no. 8, Aug. 2016, Art. no. 640, doi: 10.3390/rs8080640.

[25] E. Robert et al., "Monitoring water turbidity and surface suspended sediment concentration of the Bagre Reservoir (Burkina Faso) using MODIS and field reflectance data," *Int. J. Appl. Earth Observ. Geoinf.*, vol. 52, pp. 243–251, Oct. 2016, doi: 10.1016/j.jag.2016.06.016.

[26] J. Bratby, "Turbidity: Measurement of filtrate and supernatant quality?," in *Progress in Filtration and Separation*. Amsterdam, The Netherlands: Elsevier, 2015, pp. 637–657, doi: 10.1016/B978-0-12-384746-1.00016-1.

[27] World Health Organization, *Guidelines for Drinking-Water Quality: Fourth Edition Incorporating First Addendum*, 4th ed. Geneva, Switzerland: World Health Org., 2017, Accessed on: Jun. 15, 2023. [Online]. Available: https://apps.who.int/iris/handle/10665/254637

[28] I. Ogashawara, D. R. Mishra, and A. A. Gitelson, "Remote sensing of inland waters: Background and current state-of-the-art," in *Bio-Optical Modeling and Remote Sensing of Inland Waters*. Amsterdam, The Netherlands: Elsevier, 2017, pp. 1–24, doi: 10.1016/B978-0-12-804644-9.00001-X.

[29] R. Doerffer and H. Schiller, "The MERIS case 2 water algorithm," *Int. J. Remote Sens.*, vol. 28, no. 3/4, pp. 517–535, Feb. 2007, doi: 10.1080/01431160600821127.

[30] C. Brockmann, R. Doerffer, M. Peters, K. Stelzer, S. Embacher, and A. Ruescas, "Evolution of the C2RCC neural network for Sentinel 2 and 3 for the retrieval of ocean colour products in normal and extreme optically complex waters," in *Proc. Living Planet Symp.*, Prague, Czech Republic, May 2016, Accessed on: Jun. 8, 2023. [Online]. Available: https://www.brockmann-consult.de/wp-content/uploads/2017/11/sco1_12brockmann.pdf

[31] I. Caballero, F. Steinmetz, and G. Navarro, "Evaluation of the first year of operational sentinel-2A data for retrieval of suspended solids in medium- to high-turbidity waters," *Remote Sens.*, vol. 10, no. 7, Jun. 2018, Art. no. 982, doi: 10.3390/rs10070982.

[32] Y. Ma et al., "Remote sensing of turbidity for lakes in northeast China using Sentinel-2 images with machine learning algorithms," *IEEE J. Sel. Topics Appl. Earth Observ. Remote Sens.*, vol. 14, pp. 9132–9146, Sep. 2021, doi: 10.1109/JSTARS.2021.3109292.

[33] H. Liu et al., "Eutrophication monitoring of lakes in Wuhan based on Sentinel-2 data," *GIScience Remote Sens.*, vol. 58, no. 5, pp. 776–798, Jul. 2021, doi: 10.1080/15481603.2021.1940738.

[34] S. Heddam, "Secchi disk depth estimation from water quality parameters: Artificial neural network versus multiple linear regression models?," *Environ. Process.*, vol. 3, no. 2, pp. 525–536, Jun. 2016, doi: 10.1007/s40710-016-0144-4.

[35] A. Bhardwaj et al., "Smart IoT and machine learning-based framework for water quality assessment and device component monitoring," *Environ. Sci. Pollut. Res.*, vol. 29, no. 30, pp. 46018–46036, Jun. 2022, doi: 10.1007/s11356-022-19014-3.

[36] C. Corbari, N. Paciolla, I. Ben Charfi, D. Skokovic, J. A. Sobrino, and M. Woods, "Citizen science supporting agricultural monitoring with hundreds of low-cost sensors in comparison to remote sensing data," *Eur. J. Remote Sens.*, vol. 55, no. 1, pp. 388–408, Dec. 2022, doi: 10.1080/22797254.2022.2084643.

[37] P. Elias et al., "Mapping the landscape of citizen science in Africa: Assessing its potential contributions to sustainable development goals 6 and 11 on access to clean water and sanitation and sustainable cities," *Citizen Sci. Theory Pract.*, vol. 8, no. 1, Jun. 2023, Art. no. 33, doi: 10.5334/cstp.601.

[38] F. Mao, K. Khamis, S. Krause, J. Clark, and D. M. Hannah, "Low-cost environmental sensor networks: Recent advances and future directions," *Front. Earth Sci.*, vol. 7, Sep. 2019, Art. no. 221, doi: 10.3389/feart.2019.00221.

[39] A. Abera et al., "Air pollution measurements and land-use regression in urban sub-Saharan Africa Using low-cost sensors—Possibilities and pitfalls," *Atmosphere*, vol. 11, no. 12, Dec. 2020, Art. no. 1357, doi: 10.3390/atmos11121357.

[40] E. T. De Camargo et al., "Low-cost water quality sensors for IoT: A systematic review," *Sensors*, vol. 23, no. 9, Apr. 2023, Art. no. 4424, doi: 10.3390/s23094424.

[41] I. M. Hakimi and Z. Jamil, "Development of water quality monitoring device using Arduino UNO," *IOP Conf. Ser., Mater. Sci. Eng.*, vol. 1144, no. 1, May 2021, Art. no. 012064, doi: 10.1088/1757-899X/1144/1/012064.

[42] A. Oelen, C. J. van Aart, and V. De Boer, "Measuring surface water quality using a low-cost sensor kit within the context of rural Africa," in P-ICT4D@ WebSci, Amsterdam, The Netherlands, May 2018. [Online]. Available: https://ceur-ws.org/Vol-2120/paper3.pdf

[43] J. Trevathan, W. Read, and S. Schmidtke, "Towards the development of an affordable and practical light attenuation turbidity sensor for remote near real-time aquatic monitoring," *Sensors*, vol. 20, no. 7, Apr. 2020, Art. no. 1993, doi: 10.3390/s20071993.

[44] T. J. Malthus, R. Ohmsen, and H. J. van der Woerd, "An evaluation of citizen science smartphone apps for inland water quality assessment," *Remote Sens.*, vol. 12, no. 10, May 2020, Art. no. 1578, doi: 10.3390/rs12101578.

[45] O. O. Nathan, N. K. Felix, K. N. Milka, M. Anne, A. Noah, and M. N. Daniel, "Suitability of different data sources in rainfall pattern characterization in the tropical central highlands of Kenya," *Heliyon*, vol. 6, no. 10, Oct. 2020, Art. no. e05375, doi: 10.1016/j.heliyon.2020.e05375.

[46] S. W. Muthee et al., "Using SWAT to model the response of evapotranspiration and runoff to varying land uses and climatic conditions in the Muringato basin, Kenya," *Model. Earth Syst. Environ.*, vol. 9, pp. 1531–1543, 2023, doi: 10.1007/s40808-022-01579-0.

[47] Muringato Water Resource Users Association (WRUA), "Report on the baseline mapping and documentation of Muringato WRUA subcatchment characteristics—Basic inventory," Dedan Kimathi Univ. Technol., Nyeri, Kenya, Feb. 2018.

[48] N. Mwangi, H. Waithaka, C. Mundia, M. Kinyanjui, and F. Mutua, "Assessment of drivers of forest changes using multitemporal analysis and boosted regression trees model: A case study of Nyeri County, Central Region of Kenya," *Model. Earth Syst. Environ.*, vol. 6, no. 3, pp. 1657–1670, Sep. 2020, doi: 10.1007/s40808-020-00781-2.

[49] M. Goebel, K. Thiongo, and A. Rienow, "Object-based mapping and classification features for tropical highlands using on Sentinel-1, Sentinel-2, and GEDI canopy height data—A case study of the Muringato catchment, Kenya," *Erdkunde*, vol. 77, no. 1, pp. 35–52, 2023, doi: 10.3112/erdkunde.2023.01.03.

[50] W. Kipkemboi et al., "Development of a web-GIS platform for environmental monitoring and conservation of the Muringato catchment in Kenya," *J. Geovisualization Spatial Anal.*, vol. 7, no. 1, Jun. 2023, Art. no. 13, doi: 10.1007/s41651-023-00143-3.

[51] Government of Kenya, Ministry of Water and Irrigation, *The Water Act 2016*, 2016, Accessed on: Aug. 5, 2023. [Online]. Available: https://wasreb.go.ke/downloads/Water%20Act%202016.pdf

[52] M. Bonansea et al., "Evaluating the feasibility of using Sentinel-2 imagery for water clarity assessment in a reservoir," *J. South Amer. Earth Sci.*, vol. 95, Nov. 2019, Art. no. 102265, doi: 10.1016/j.jsames.2019.102265.

[53] M. A. Warren et al., "Assessment of atmospheric correction algorithms for the Sentinel-2A MultiSpectral imager over coastal and inland waters," *Remote Sens. Environ.*, vol. 225, pp. 267–289, May 2019, doi: 10.1016/j.rse.2019.03.018.

[54] C. B. Mouw et al., "Aquatic color radiometry remote sensing of coastal and inland waters: Challenges and recommendations for future satellite missions," *Remote Sens. Environ.*, vol. 160, pp. 15–30, Apr. 2015, doi: 10.1016/j.rse.2015.02.001.

[55] S. Li et al., "Performances of atmospheric correction processors for sentinel-2 MSI imagery over typical lakes across China," *IEEE J. Sel. Topics Appl. Earth Observ. Remote Sens.*, vol. 16, pp. 2065–2078, Jan. 2023, doi: 10.1109/JSTARS.2023.3238713.

[56] X. Sun et al., "Monitoring water quality using proximal remote sensing technology," *Sci. Total Environ.*, vol. 803, Jan. 2022, Art. no. 149805, doi: 10.1016/j.scitotenv.2021.149805.

[57] M. H. Tavares, R. C. Lins, T. Harmel, C. R. Fragoso, Jr, J.-M. Martínez, and D. Motta-Marques, "Atmospheric and sunglint correction for retrieving chlorophyll-a in a productive tropical Estuarine-Lagoon System using Sentinel-2 MSI imagery," *ISPRS J. Photogramm. Remote Sens.*, vol. 174, pp. 215–236, Apr. 2021, doi: 10.1016/j.isprsjprs.2021.01.021.

[58] Garmin, "ETREX 22X/32X owner's manual," 2020, Accessed on: Apr. 13, 2023. [Online]. Available: https://www8.garmin.com/manuals/webhelp/eTrex22x-32x/EN-US/eTrex_22x_32x_OM_EN-US.pdf

[59] Lovibond Water Testing, "TB 211 IR datasheet," 2021, Accessed on: Jun. 2, 2023. [Online]. Available: https://www.lovibond.com/ix_pim_assets/datasheet/water/en/Datasheet%20266030%20-%20TB%20211%20IR%20en.pdf

[60] DFRobot, "Turbidity sensor SKU: SEN0189," 2017, Accessed on: Jun. 2, 2023. [Online]. Available: https://media.digikey.com/pdf/data%20sheets/dfrobot%20pdfs/sen0189_web.pdf

[61] Thermometrics, "TSW-10 turbidity sensor," 2019, Accessed on: Jun. 2, 2023. [Online]. Available: https://f.hubspotusercontent40.net/hubfs/9035299/AAS-920-479C-Thermometrics-TSW-10-100919-web.pdf

[62] W. D. Kirkey, J. S. Bonner, and C. B. Fuller, "Low-cost submersible turbidity sensors using low-frequency source light modulation," *IEEE Sensors J.*, vol. 18, no. 22, pp. 9151–9162, Nov. 2018, doi: 10.1109/JSEN.2018.2869368.

[63] D. Petrov, K.-F. Taron, U. Hilleringmann, and T.-H. Joubert, "Low-cost sensor system for on-the-field water quality analysis," in *Proc. Smart Syst. Integr.*, 2021, pp. 1–4, doi: 10.1109/SSI52265.2021.9466956.

[64] A. Morel and L. Prieur, "Analysis of variations in ocean color1: Ocean color analysis," *Limnol. Oceanogr.*, vol. 22, no. 4, pp. 709–722, Jul. 1977, doi: 10.4319/lo.1977.22.4.0709.

[65] D. Odermatt, A. Gitelson, V. E. Brando, and M. Schaepman, "Review of constituent retrieval in optically deep and complex waters from satellite imagery," *Remote Sens. Environ.*, vol. 118, pp. 116–126, Mar. 2012, doi: 10.1016/j.rse.2011.11.013.

[66] A. A. Gitelson and K. Y. Kondratyev, "Optical models of mesotrophic and eutrophic water bodies," *Int. J. Remote Sens.*, vol. 12, no. 3, pp. 373–385, Mar. 1991, doi: 10.1080/01431169108929659.

[67] H. R. Gordon and W. R. McCluney, "Estimation of the depth of sunlight penetration in the sea for remote sensing," *Appl. Opt.*, vol. 14, no. 2, pp. 413–416, Feb. 1975, doi: 10.1364/AO.14.000413.

[68] K. Uudeberg, I. Ansko, G. Põru, A. Ansper, and A. Reinart, "Using optical water types to monitor changes in optically complex inland and coastal waters," *Remote Sens.*, vol. 11, no. 19, Oct. 2019, Art. no. 2297, doi: 10.3390/rs11192297.

[69] A. Cuartero, J. Cáceres-Merino, and J. A. Torrecilla-Pinero, "An application of C2-net atmospheric corrections for chlorophyll-a estimation in small reservoirs," *Remote Sens. Appl. Soc. Environ.*, vol. 32, Nov. 2023, Art. no. 101021, doi: 10.1016/j.rsase.2023.101021.

[70] M. Niroumand-Jadidi, F. Bovolo, L. Bruzzone, and P. Gege, "Inter-comparison of methods for chlorophyll-a retrieval: Sentinel-2 time-series analysis in Italian lakes," *Remote Sens.*, vol. 13, no. 12, Jun. 2021, Art. no. 2381, doi: 10.3390/rs13122381.

[71] J. Tavora et al., "Recipes for the derivation of water quality parameters using the high-spatial-resolution data from sensors on board sentinel-2A, sentinel-2B, Landsat-5, Landsat-7, Landsat-8, and Landsat-9 satellites," *J. Remote Sens.*, vol. 3, Jan. 2023, Art. no. 0049, doi: 10.34133/remotesensing.0049.

[72] M. Lock, N. Saintilan, I. van Duren, and A. Skidmore, "Monitoring coastal water body health with Sentinel-2 MSI imagery," *Remote Sens.*, vol. 15, no. 7, Mar. 2023, Art. no. 1734, doi: 10.3390/rs15071734.

[73] J. F. Toro Herrera, D. Carrion, M. Bresciani, and G. Bratić, "Semi-automated production and filtering of satellite derived water quality parameters," *Int. Arch. Photogramm., Remote Sens. Spatial Inf. Sci.*, vol. XLIII-B3-2022, pp. 1019–1026, May 2022, doi: 10.5194/isprs-archives-XLIII-B3-2022-1019-2022.

[74] M. Bresciani et al., "Monitoring water quality in two dammed reservoirs from multispectral satellite data," *Eur. J. Remote Sens.*, vol. 52, no. sup4, pp. 113–122, Dec. 2019, doi: 10.1080/22797254.2019.1686956.

[75] N. Gorelick, M. Hancher, M. Dixon, S. Ilyushchenko, D. Thau, and R. Moore, "Google Earth engine: Planetary-scale geospatial analysis for everyone," *Remote Sens. Environ.*, vol. 202, pp. 18–27, Dec. 2017, doi: 10.1016/j.rse.2017.06.031.

[76] M. Drusch et al., "Sentinel-2: ESA's optical high-resolution mission for GMES operational services," *Remote Sens. Environ.*, vol. 120, pp. 25–36, May 2012, doi: 10.1016/j.rse.2011.11.026.

[77] T. G. Farr et al., "The shuttle radar topography mission," *Rev. Geophys.*, vol. 45, no. 2, May 2007, Art. no. RG2004, doi: 10.1029/2005RG000183.

[78] E. Kalnay et al., "The NCEP/NCAR 40-year reanalysis project," *Bull. Amer. Meteorol. Soc.*, vol. 77, no. 3, pp. 437–472, Mar. 1996, doi: 10.1175/1520-0477(1996)077%3C0437:TNYRP%3E2.0.CO;2.

[79] R. McPeters et al., "Total ozone mapping spectrometer (TOMS) level-3 data products user's guide," Nat. Aeronaut. Space Admin., Greenbelt, MD, USA, Jul. 2000.

[80] Y. Zhang et al., "Improving remote sensing estimation of Secchi disk depth for global lakes and reservoirs using machine learning methods," *GIScience Remote Sens.*, vol. 59, no. 1, pp. 1367–1383, Dec. 2022, doi: 10.1080/15481603.2022.2116102.

[81] D. Chicco, M. J. Warrens, and G. Jurman, "The coefficient of determination R-squared is more informative than SMAPE, MAE, MAPE, MSE and RMSE in regression analysis evaluation," *PeerJ Comput. Sci.*, vol. 7, Jul. 2021, Art. no. e623, doi: 10.7717/peerj-cs.623.

[82] KEBS, "Kenya Standard (KS EAS 12: 2014, First Edition) specifications for potable water," Kenya Bureau of Standards (KEBS), Nairobi, Kenya, 2015, Accessed on: Jun. 15, 2023. [Online]. Available: https://academicjournals.org/journal/IJWREE/article-full-text-pdf/03934C661299

[83] M. Bresciani et al., "Analysis of within- and between-day chlorophyll-a dynamics in Mantua Superior Lake, with a continuous spectroradiometric measurement," *Mar. Freshwater Res.*, vol. 64, no. 4, 2013, Art. no. 303, doi: 10.1071/MF12229.

[84] S. C. J. Palmer, T. Kutser, and P. D. Hunter, "Remote sensing of inland waters: Challenges, progress and future directions," *Remote Sens. Environ.*, vol. 157, pp. 1–8, Feb. 2015, doi: 10.1016/j.rse.2014.09.021.
[85] D. Jiang et al., "A data-driven approach to flag land-affected signals in satellite derived water quality from small lakes," *Int. J. Appl. Earth Observ. Geoinf.*, vol. 117, Mar. 2023, Art. no. 103188, doi: 10.1016/j.jag.2023.103188.
[86] R. S. Paulino, V. S. Martins, E. M. L. M. Novo, C. C. F. Barbosa, L. A. S. De Carvalho, and F. N. Begliomini, "Assessment of adjacency correction over inland waters using Sentinel-2 MSI images," *Remote Sens.*, vol. 14, no. 8, Apr. 2022, Art. no. 1829, doi: 10.3390/rs14081829.
[87] "Global and national soils and terrain databases (SOTER)—Procedures manual," ISRIC - World Soil Information, Wageningen, The Netherlands, 2013, Accessed on: Feb. 17, 2023. [Online]. Available: https://www.isric.org/sites/default/files/isric_report_2013_04.pdf
[88] S. Hafeez et al., "Comparison of machine learning algorithms for retrieval of water quality indicators in case-II waters: A case study of Hong Kong," *Remote Sens.*, vol. 11, no. 6, Mar. 2019, Art. no. 617, doi: 10.3390/rs11060617.
[89] S. Zhang et al., "Evaluating atmospheric correction methods for sentinel−2 in low−to−high−turbidity Chinese coastal waters," *Remote Sens.*, vol. 15, no. 9, Apr. 2023, Art. no. 2353, doi: 10.3390/rs15092353.
[90] D. Gillett and A. Marchiori, "A low-cost continuous turbidity monitor," *Sensors*, vol. 19, no. 14, Jul. 2019, Art. no. 3039, doi: 10.3390/s19143039.
[91] B. T. W. Putra, L. A. Rocelline, and W. N. H. Syahputra, "Embedded system in handheld water turbidity meter for smallholders," *Microprocessors Microsyst.*, vol. 93, Sep. 2022, Art. no. 104603, doi: 10.1016/j.micpro.2022.104603.
[92] J. Droujko and P. Molnar, "Open-source, low-cost, in-situ turbidity sensor for river network monitoring," *Sci. Rep.*, vol. 12, no. 1, Jun. 2022, Art. no. 10341, doi: 10.1038/s41598-022-14228-4.
[93] K. R. Smith et al., "Clustering approaches to improve the performance of low cost air pollution sensors," *Faraday Discuss.*, vol. 200, pp. 621–637, 2017, doi: 10.1039/C7FD00020K.
[94] Department of Water Affairs and Forestry, *South African Water Quality Guidelines—Agricultural Water Use: Livestock Watering*, vol. 5. 2nd ed., Dept. Water Affairs Forestry, Pretoria, South Africa, 1996. [Online]. Available: https://www.dws.gov.za/iwqs/wq_guide/edited/Pol_saWQguideFRESH_vol5_Livestockwatering.pdf
[95] D. Nukpezah, F. A. Rahman, and S. S. Koranteng, "The impact of small scale mining on irrigation water quality in Asante Akim central municipality of Ghana," *West Afr. J. Appl. Ecol.*, vol. 25, pp. 49–67, 2017.
[96] M. Pompêo, V. Moschini-Carlos, M. D. Bitencourt, X. Sòria-Perpinyà, E. Vicente, and J. Delegido, "Water quality assessment using Sentinel-2 imagery with estimates of chlorophyll a, Secchi disk depth, and cyanobacteria cell number: The Cantareira system reservoirs (São Paulo, Brazil)," *Environ. Sci. Pollut. Res.*, vol. 28, no. 26, pp. 34990–35011, Jul. 2021, doi: 10.1007/s11356-021-12975-x.
[97] R. Quinn, O. Avis, M. Decker, A. Parker, and S. Cairncross, "An assessment of the microbiological water quality of sand dams in southeastern Kenya," *Water*, vol. 10, no. 6, May 2018, Art. no. 708, doi: 10.3390/w10060708.
[98] K. T. Peterson, V. Sagan, and J. J. Sloan, "Deep learning-based water quality estimation and anomaly detection using Landsat-8/Sentinel-2 virtual constellation and cloud computing," *GIScience Remote Sens.*, vol. 57, no. 4, pp. 510–525, May 2020, doi: 10.1080/15481603.2020.1738061.
[99] H. Jepleting, J. Mulei, J. E. Chemoiwa, J. Barasa, J. Wanga, and C. Saina, "Influence of water quality on distribution patterns and diversity of Enteromius fish species in small water bodies of Uasin Gishu county, Kenya," *Afr. J. Educ., Sci. Technol.*, vol. 7, no. 2, pp. 1–20, Nov. 2022, doi: 10.2022/ajest.v7i2.797.
[100] S. G. P. Virdis, W. Xue, E. Winijkul, V. Nitivattananon, and P. Punpukdee, "Remote sensing of tropical riverine water quality using Sentinel-2 MSI and field observations," *Ecol. Indicators*, vol. 144, Nov. 2022, Art. no. 109472, doi: 10.1016/j.ecolind.2022.109472.
[101] M. Langensiepen et al., "Reconciling East-African wetland conservation with human needs: Managing uncertainties in environmental policy design," *Wetlands*, vol. 43, no. 4, Apr. 2023, Art. no. 36, doi: 10.1007/s13157-023-01679-2.
[102] M. Chowdhury, C. Vilas, S. van Bergeijk, G. Navarro, I. Laiz, and I. Caballero, "Monitoring turbidity in a highly variable estuary using Sentinel 2-A/B for ecosystem management applications," *Front. Mar. Sci.*, vol. 10, Jul. 2023, Art. no. 1186441, doi: 10.3389/fmars.2023.1186441.
[103] R. Ajates, G. Hager, P. Georgiadis, S. Coulson, M. Woods, and D. Hemment, "Local action with global impact: The case of the grow observatory and the sustainable development goals," *Sustainability*, vol. 12, no. 24, Dec. 2020, Art. no. 10518, doi: 10.3390/su122410518.
[104] J. Hadj-Hammou, S. Loiselle, D. Ophof, and I. Thornhill, "Getting the full picture: Assessing the complementarity of citizen science and agency monitoring data," *PLoS One*, vol. 12, no. 12, Dec. 2017, Art. no. e0188507, doi: 10.1371/journal.pone.0188507.
[105] I. Dronova, P. Gong, L. Wang, and L. Zhong, "Mapping dynamic cover types in a large seasonally flooded wetland using extended principal component analysis and object-based classification," *Remote Sens. Environ.*, vol. 158, pp. 193–206, Mar. 2015, doi: 10.1016/j.rse.2014.10.027.
[106] S. Mahdavi, B. Salehi, J. Granger, M. Amani, B. Brisco, and W. Huang, "Remote sensing for wetland classification: A comprehensive review," *GIScience Remote Sens.*, vol. 55, no. 5, pp. 623–658, Sep. 2018, doi: 10.1080/15481603.2017.1419602.
[107] J. Muro, A. Strauch, E. Fitoka, M. Tompoulidou, and F. Thonfeld, "Mapping wetland dynamics with SAR-based change detection in the cloud," *IEEE Geosci. Remote Sens. Lett.*, vol. 16, no. 10, pp. 1536–1539, Oct. 2019, doi: 10.1109/LGRS.2019.2903596.
[108] K. H. Thamaga and T. Dube, "Understanding seasonal dynamics of invasive water hyacinth (Eichhornia crassipes) in the Greater Letaba river system using Sentinel-2 satellite data," *GIScience Remote Sens.*, vol. 56, no. 8, pp. 1355–1377, Nov. 2019, doi: 10.1080/15481603.2019.1646988.
[109] K. Weise et al., "Wetland extent tools for SDG 6.6.1 reporting from the satellite-based wetland observation service (SWOS)," *Remote Sens. Environ.*, vol. 247, Sep. 2020, Art. no. 111892, doi: 10.1016/j.rse.2020.111892.
[110] M. Mleczko, M. Mroz, and M. Fitrzyk, "Riparian wetland mapping and inundation monitoring using amplitude and bistatic coherence data from the TanDEM-X mission," *IEEE J. Sel. Topics Appl. Earth Observ. Remote Sens.*, vol. 14, pp. 2432–2444, Jan. 2021, doi: 10.1109/JSTARS.2021.3109292.
[111] X. Zhang, S. Fu, Z. Hu, J. Zhou, and X. Zhang, "Changes detection and object-oriented classification of major wetland cover types in response to driving forces in Zoige County, Eastern Qinghai–Tibetan Plateau," *IEEE J. Sel. Topics Appl. Earth Observ. Remote Sens.*, vol. 14, pp. 9297–9305, Aug. 2021, doi: 10.1109/JSTARS.2021.3104223.
[112] S. Steinbach et al., "A new conceptual framework for integrating earth observation in large-scale wetland management in East Africa," *Wetlands*, vol. 41, no. 7, Oct. 2021, Art. no. 93, doi: 10.1007/s13157-021-01468-9.
[113] S. Steinbach et al., "Automatization and evaluation of a remote sensing-based indicator for wetland health assessment in East Africa on national and local scales," *Ecol. Inform.*, vol. 75, Jul. 2023, Art. no. 102032, doi: 10.1016/j.ecoinf.2023.102032.
[114] S. Beuel et al., "A rapid assessment of anthropogenic disturbances in East African wetlands," *Ecol. Indicators*, vol. 67, pp. 684–692, Aug. 2016, doi: 10.1016/j.ecolind.2016.03.034.
[115] M. D'Alessio, G. Rushing, and T. L. Gray, "Monitoring water quality through citizen science while teaching STEM undergraduate courses during a global pandemic," *Sci. Total Environ.*, vol. 779, Jul. 2021, Art. no. 146547, doi: 10.1016/j.scitotenv.2021.146547.
[116] H. Hodam, A. Rienow, and C. Juergens, "Developing and evaluating simplified tools for image processing in a problem-based learning environment for Earth observation," *PFG – J. Photogramm. Remote Sens. Geoinf. Sci.*, vol. 90, no. 5, pp. 439–456, Oct. 2022, doi: 10.1007/s41064-022-00211-1.
[117] C. Lindner, A. Rienow, K.-H. Otto, and C. Juergens, "Development of an app and teaching concept for implementation of hyperspectral remote sensing data into school lessons using augmented reality," *Remote Sens.*, vol. 14, no. 3, Feb. 2022, Art. no. 791, doi: 10.3390/rs14030791.
[118] A. R. Ignatius et al., "Water in geospatial higher education: A discussion of lessons learned," in *Proc. Georgia Water Resour. Conf.*, 2021, pp. 1–8.

Stefanie Steinbach is currently working toward the Ph.D. degree in geo-information science and Earth observation with the International Institute for Geo-Information Science and Earth Observation (ITC), University of Twente, Enschede, The Netherlands.

She is a Researcher with Ruhr University Bochum, Bochum, Germany. Her focus is on Earth observation tools for the sustainable management of natural resources in a food security context.

Andreas Rienow received the Ph.D. degree in geography from Rheinische Friedrich Wilhelms University, Bonn, Germany, in 2014.

He is a junior Professor and the Head of the Interdisciplinary Geoinformation Sciences Group, Ruhr University Bochum, Bochum, Germany. In addition, he has been the Scientific Director of the Interdisciplinary Center for Geoinformation, Ruhr University Bochum, since 2020. His foci are the spatiotemporal analysis of the transformation of metropolitan spaces, the interdisciplinary integration of geodata, Earth observation education, and the analysis of real-time geoinformation.

Martin Wainaina Chege is currently working toward the master's degree in geospatial information systems and remote sensing with the Dedan Kimathi University of Technology, Nyeri, Kenya.

He works with the Remote Sensing Research Group, Institute of Geomatics, GIS and Remote Sensing, Nyeri, Kenya. His research focus includes low-cost sensor system development, GIS development, Earth observation, and hydrological modeling.

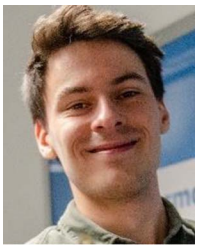

Niels Dedring is currently working toward the master's degree in geography with the Ruhr University of Bochum, Bochum, Germany.

He works with the Interdisciplinary Geographic Information Sciences Research Group, Institute of Geography, Ruhr University of Bochum, Germany. His research focus includes low-cost sensors for environmental and agricultural monitoring and modeling of natural hazards using remote sensing data.

Wisdom Kipkemboi received the M.Sc. degree in geospatial information systems and remote sensing from the Dedan Kimathi University of Technology, Nyeri, Kenya, in 2023.

He works with the Institute of Geomatics, GIS and Remote Sensing, Dedan Kimathi University of Technology, Nyeri, Kenya, and is a member of Remote Sensing Research Group. His research interests include Earth observation, GIS development, and citizen science and participatory GIS.

Bartholomew Kuria Thiong'o received the Ph.D. degree in natural sciences from Ruhr University Bochum, Bochum, Germany, in 2018.

He is a Researcher with the Institute of Geomatics, GIS and Remote Sensing, Dedan Kimathi University of Technology, Nyeri, Kenya, and the Head of Remote Sensing Research Group, conducting research on geoinformation for land use, socioeconomic assessments, food security, natural resources management, and integrated geoinformation and participatory approaches.

Sander Jaap Zwart received the Ph.D. degree in water productivity from the Delft University of Technology, Delft, The Netherlands, in 2010.

He is a Researcher with the International Water Management Institute, Accra, Ghana, working in the fields of irrigation, remote sensing, water solutions, climate change, and water resources assessment.

Andrew Nelson received the Ph.D. degree in geography from the University of Leeds, Leeds, U.K., in 2004.

He is a Professor of spatial agriculture and food security with the Faculty of Geo-Information Science and Earth Observation (ITC), University of Twente, Enschede, The Netherlands. He has conducted spatial research on a wide range of natural resource and agricultural issues within the CGIAR, the World Bank, FAO, UNEP, and the European Commission.